Definitive Thermochemistry and Kinetics of the Interconversions among Conformers of *n*-Butane and *n*-Pentane

Roland Tóbiás [a], Attila G. Császár *[a,b], László Gyevi-Nagy,[c] and Gyula Tasi*[d]

The focal-point analysis (FPA) technique is used for the definitive characterization of conformational interconversion parameters, including activation energy barriers, activation free energies, and kinetic rate coefficients at 298 K, of two *n*-alkanes, *n*-butane, and *n*-pentane, yielding the first complete analysis of their interconversion kinetics. The FPA implementation developed in this study is based on geometry optimizations and harmonic frequency computations carried out with density functional theory methods and single-point energy computations up to the CCSD(T) level of electronic structure theory using atom-centered Gaussian basis sets as large as cc-pV5Z. The anharmonic vibrational computations are carried out, at the MP2/6-31G* level of theory. Reflecting the convergence behavior of the Gibbs free-energy terms and the interconversion parameters, well-defined uncertainties, mostly neglected in previous theoretical studies, are provided. Finally, the effect of these uncertainties on the concentrations of the conformers of *n*-butane and *n*-pentane is examined via a global Monte–Carlo uncertainty analysis.

DOI: 10.1002/jcc.25130

Introduction

Normal alkanes are among the simplest molecules of importance for organic chemistry. Due to the presence of a number of CC single bonds, *n*-alkanes exhibit considerable conformational flexibility. A comprehensive description of the conformational behavior of *n*-alkanes helps to understand the allowed conformational space of more complicated and complex organic compounds, like lipids, polymers, proteins, and nucleic acids. Therefore, it is not surprising that several experimental and theoretical studies have appeared with the aim to (a) explore the stationary (critical) points on the conformational potential energy surfaces (CPES) of *n*-alkanes[1] and other flexible molecules[2–9]; (b) investigate the energetics and the conformational equilibria of the conformers[10–30]; and (c) determine kinetic parameters describing the interconversions among the conformers.[31–40] The best experimental studies[3,13,24,31–40] utilized several spectroscopic (infrared, ultraviolet, and Raman) techniques, while the best theoretical studies[4–8,16,19–22,25,27,29,36] applied variants of the focal-point analysis (FPA) approach,[41,42] within which particularly accurate results with well-defined uncertainties can be obtained for energy differences of the critical points.

Any point on the CPES of a *n*-alkane with n_C carbon atoms can be identified by n_C-3 CCCC (backbone) torsion angles. The structure of the backbone dihedral angles $\Theta_1, \Theta_2, \ldots, \Theta_{n_C-3}$ is denoted here by a torsion sequence $\Lambda(\Theta_1)\Lambda(\Theta_2)\ldots\Lambda(\Theta_{n_C-3})$, where $\Lambda(\Theta_i)$ is a label based on the value of $\Theta_i \in (-\pi, \pi]$. It is known[43,44] that the following four torsion sequences have the same physical properties:

$$\begin{aligned} s_1 &= \Lambda(\Theta_1)\Lambda(\Theta_2)\ldots\Lambda(\Theta_{n_C-3}) \\ s_2 &= \Lambda(\Theta_{n_C-3})\ldots\Lambda(\Theta_2)\Lambda(\Theta_1) \\ s_3 &= \Lambda(-\Theta_1)\Lambda(-\Theta_2)\ldots\Lambda(-\Theta_{n_C-3}) \\ s_4 &= \Lambda(-\Theta_{n_C-3})\ldots\Lambda(-\Theta_2)\Lambda(-\Theta_1), \end{aligned} \quad (1)$$

which are called isomorphic torsion sequences. As a result, isomorphic *n*-alkane conformers are indistinguishable via spectroscopic measurements. Isomorphic torsion sequences can be divided into equivalence classes. Each equivalence class is well represented with one of its entries, called a unique sequence (structure).

[a] *R. Tóbiás, A. G. Császár*
MTA-ELTE Complex Chemical Systems Research Group, H-1518 Budapest 112, P.O. Box 32, Hungary
E-mail: csaszar@chem.elte.hu
[b] *A. G. Császár*
Laboratory of Molecular Structure and Dynamics, Institute of Chemistry, Eötvös Loránd University, H-1117 Budapest, Pázmány Péter sétány 1/A, Hungary
[c] *L. Gyevi-Nagy*
Department of Physical Chemistry and Materials Science, University of Szeged, H-6720 Szeged, Rerrich B. tér 1, Hungary
[d] *G. Tasi*
Department of Applied and Environmental Chemistry, University of Szeged, H-6720 Szeged, Rerrich B. tér 1, Hungary
E-mail: tasi@chem.u-szeged.hu
Contract grant sponsor: NKFIH; Contract grant number: K119658

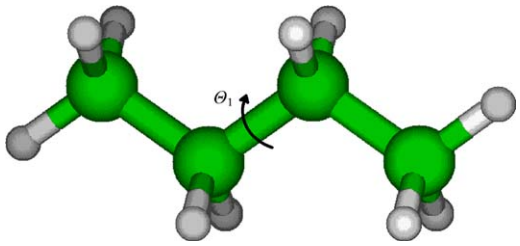

Figure 1. Backbone torsional angle (Θ_1) in *n*-butane, along which the (conformational) interconversions take place. [Color figure can be viewed at wileyonlinelibrary.com]

The smallest *n*-alkane exhibiting rotational isomerism is *n*-butane. The one-dimensional CPES of this molecule can be mapped by varying a single torsion angle, for example, Θ_1 in Figure 1, while relaxing all the other internal coordinates. It is well established[45] that the CPES of *n*-butane has three minima, corresponding to three conformers, with the labels $\Lambda(\approx 180^\circ) \equiv \mathrm{t}$, $\Lambda(\approx 60^\circ) \equiv \mathrm{g}^+$, and $\Lambda(\approx -60^\circ) \equiv \mathrm{g}^-$, and three transition states with $\Lambda(\approx 0^\circ) \equiv \tau$, $\Lambda(\approx 120^\circ) \equiv \xi^+$, and $\Lambda(\approx -120^\circ) \equiv \xi^-$. These conformers and transition states define the following sequences of interconversions:

$$\begin{aligned} &\mathrm{t}[\rightleftharpoons\xi^+]\rightleftharpoons\mathrm{g}^+,\\ &\mathrm{t}[\rightleftharpoons\xi^-]\rightleftharpoons\mathrm{g}^-,\\ &\mathrm{g}^+[\rightleftharpoons\tau]\rightleftharpoons\mathrm{g}^-, \end{aligned} \tag{2}$$

where the transition states are indicated in brackets. The minima and the transition states of the CPES related to *n*-butane can be divided into the classes $c_1=\{\mathrm{t}\}$, $c_2=\{\mathrm{g}^+,\mathrm{g}^-\}$, $c_3=\{\tau\}$, and $c_4=\{\xi^+,\xi^-\}$, whose unique critical points are represented by t, $\mathrm{g}^\pm$, τ, and $\xi^\pm$. Therefore, eq. (2) can be reduced to

$$\begin{aligned} &\mathrm{t}[\rightleftharpoons\xi^\pm]\rightleftharpoons\mathrm{g}^\pm\\ &\mathrm{g}^\pm[\rightleftharpoons\tau]\rightleftharpoons\mathrm{g}^\pm, \end{aligned} \tag{3}$$

where $\mathrm{t}[\rightleftharpoons\xi^\pm]\rightleftharpoons\mathrm{g}^\pm$ is either $\mathrm{t}[\rightleftharpoons\xi^+]\rightleftharpoons\mathrm{g}^+$ or $\mathrm{t}[\rightleftharpoons\xi^-]\rightleftharpoons\mathrm{g}^-$, and $\mathrm{g}^\pm[\rightleftharpoons\tau]\rightleftharpoons\mathrm{g}^\pm$ denotes the pair of reactions $\mathrm{g}^+[\rightleftharpoons\tau]\rightleftharpoons\mathrm{g}^-$. These processes fully describe the kinetics of eq. (2).

As to the conformational flexibility of *n*-pentane, 11 minima, 20 transition states, and 9 maxima have been established for this molecule by Tasi et al.[1] The existence of these stationary points was later confirmed by an independent study.[46] The complex CPES of *n*-pentane is defined by two torsion angles, see Θ_1 and Θ_2 of Figure 2. Among the 11 conformers the following interconversions could be identified[1]:

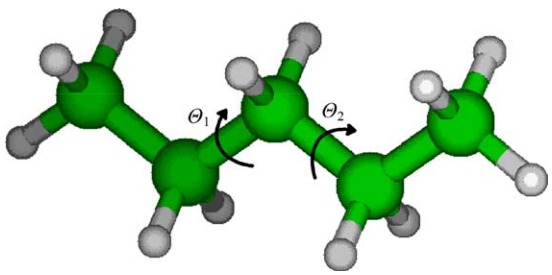

Figure 2. Backbone torsional angles (Θ_1 and Θ_2) in *n*-pentane, along which the (conformational) interconversions take place. [Color figure can be viewed at wileyonlinelibrary.com]

$$\begin{aligned}
&\mathrm{tt}[\rightleftharpoons\mathrm{t}\xi^+]\rightleftharpoons\mathrm{tg}^+ && \mathrm{tg}^+[\rightleftharpoons\xi^+\mathrm{g}^+]\rightleftharpoons\mathrm{g}^+\mathrm{g}^+\\
&\mathrm{tt}\ [\rightleftharpoons\xi^+\mathrm{t}]\rightleftharpoons\mathrm{g}^+\mathrm{t} && \mathrm{g}^+\mathrm{t}[\rightleftharpoons\mathrm{g}^+\xi^+]\rightleftharpoons\mathrm{g}^+\mathrm{g}^+\\
&\mathrm{tt}[\rightleftharpoons\mathrm{t}\xi^-]\rightleftharpoons\mathrm{tg}^- && \mathrm{tg}^-[\rightleftharpoons\xi^-\mathrm{g}^-]\rightleftharpoons\mathrm{g}^-\mathrm{g}^-\\
&\mathrm{tt}[\rightleftharpoons\xi^-\mathrm{t}]\rightleftharpoons\mathrm{g}^-\mathrm{t} && \mathrm{g}^-\mathrm{t}[\rightleftharpoons\mathrm{g}^-\xi^-]\rightleftharpoons\mathrm{g}^-\mathrm{g}^-\\
&\mathrm{tg}^+[\rightleftharpoons\xi^-\mathrm{g}^+]\rightleftharpoons\mathrm{x}^-\mathrm{g}^+ && \mathrm{g}^+\mathrm{g}^+[\rightleftharpoons\tau\mathrm{x}^-]\rightleftharpoons\mathrm{g}^+\mathrm{x}^-\\
&\mathrm{g}^+\mathrm{t}[\rightleftharpoons\mathrm{g}^+\xi^-]\rightleftharpoons\mathrm{g}^+\mathrm{x}^- && \mathrm{g}^+\mathrm{g}^+[\rightleftharpoons\mathrm{x}^-\tau]\rightleftharpoons\mathrm{x}^-\mathrm{g}^+\\
&\mathrm{tg}^-[\rightleftharpoons\xi^+\mathrm{g}^-]\rightleftharpoons\mathrm{x}^+\mathrm{g}^- && \mathrm{g}^-\mathrm{g}^-[\rightleftharpoons\tau\mathrm{x}^+]\rightleftharpoons\mathrm{g}^-\mathrm{x}^+\\
&\mathrm{g}^-\mathrm{t}[\rightleftharpoons\mathrm{g}^-\xi^+]\rightleftharpoons\mathrm{g}^-\mathrm{x}^+ && \mathrm{g}^-\mathrm{g}^-[\rightleftharpoons\mathrm{x}^+\tau]\rightleftharpoons\mathrm{x}^+\mathrm{g}^-\\
&\mathrm{tg}^+[\rightleftharpoons\mathrm{t}\tau]\rightleftharpoons\mathrm{tg}^- && \mathrm{g}^+\mathrm{x}^-[\rightleftharpoons\gamma^+\gamma^-]\rightleftharpoons\mathrm{x}^+\mathrm{g}^-\\
&\mathrm{g}^+\mathrm{t}[\rightleftharpoons\tau\mathrm{t}]\rightleftharpoons\mathrm{g}^-\mathrm{t} && \mathrm{g}^-\mathrm{x}^+[\rightleftharpoons\gamma^-\gamma^+]\rightleftharpoons\mathrm{x}^-\mathrm{g}^+,
\end{aligned} \tag{4}$$

where $\Lambda(\approx 95^\circ) \equiv \mathrm{x}^+$, $\Lambda(\approx -95^\circ) \equiv \mathrm{x}^-$, $\Lambda(\approx 75^\circ) \equiv \gamma^+$, and $\Lambda(\approx -75^\circ) \equiv \gamma^-$. Equation (4) can be simplified with the set of unique critical points {tt, $\mathrm{tg}^\pm$, $\mathrm{g}^\pm\mathrm{g}^\pm$, $\mathrm{g}^\pm\mathrm{x}^\mp$, $\gamma^\pm\gamma^\mp$, $\mathrm{t}\tau$, $\mathrm{x}^\pm\tau$, $\mathrm{t}\xi^\pm$, $\mathrm{g}^\pm\xi^\pm$, $\mathrm{g}^\pm\xi^\mp$} as follows:

$$\begin{aligned}
&\mathrm{tt}[\rightleftharpoons\mathrm{t}\xi^\pm]\rightleftharpoons\mathrm{tg}^\pm\\
&\mathrm{tg}^\pm[\rightleftharpoons\mathrm{g}^\pm\xi^\pm]\rightleftharpoons\mathrm{g}^\pm\mathrm{g}^\pm\\
&\mathrm{tg}^\pm[\rightleftharpoons\mathrm{g}^\pm\xi^\mp]\rightleftharpoons\mathrm{g}^\pm\mathrm{x}^\mp\\
&\mathrm{g}^\pm\mathrm{g}^\pm[\rightleftharpoons\mathrm{x}^\pm\tau]\rightleftharpoons\mathrm{g}^\pm\mathrm{x}^\mp\\
&\mathrm{tg}^\pm[\rightleftharpoons\mathrm{t}\tau]\rightleftharpoons\mathrm{tg}^\pm\\
&\mathrm{g}^\pm\mathrm{x}^\mp[\rightleftharpoons\gamma^\pm\gamma^\mp]\rightleftharpoons\mathrm{g}^\pm\mathrm{x}^\mp.
\end{aligned} \tag{5}$$

The conformational thermodynamics of *n*-butane was reviewed recently by two of the present authors.[27] They showed that the generally accepted experimental values for the enthalpy difference of *n*-butane are biased by the improper statistical model utilized during the evaluation of the direct experimental data. It was also demonstrated there that the thermochemical quantities estimated using state-of-art electronic structure computations within the FPA approach can compete with spectroscopic methods as far as their accuracy ($\pm$10 cal mol^{-1}) is concerned. Similar conclusions were obtained[29] by some of the coauthors of this study for the energy and enthalpy differences for the conformers of *n*-pentane.

The principal purpose of the present investigation is the formulation of an FPA protocol capable of estimating accurate interconversion rate coefficients of *n*-alkanes larger than the two alkanes of the present study. Thus, the FPA protocol to be developed must be based on inexpensive geometry optimizations and harmonic frequency computations. These computations could be carried out at the density functional theory (DFT) level of electronic structure theory. Another important aim of this study, following a recent recommendation about reporting highly accurate computational results in the field of atomic and molecular physics,[47] is the detailed uncertainty analysis of the free energy contributions, as well as the effect

of the computed uncertainties on the concentration profiles and kinetic rates of the interconversion processes.

Methodological Considerations

FPA approach

The computational techniques utilized in this study are similar to those used in Refs. [27] and [29] to benchmark the relative enthalpies of the conformers of *n*-butane and *n*-pentane. References [27] and [29] made use of the FPA approach[41,42] to provide uncertainties of sub-kJ mol^{-1} accuracy for the relative energies without making any empirical adjustments. Note that within the FPA technique the accuracy of the thermochemical quantities determined depends on the accuracy of (a) the reference structures and the harmonic frequencies; (b) the individual energy increments of the FPA scheme, which can be improved by extrapolating them to the complete basis set (CBS) limit; and (c) additional "small corrections" (relativistic effects,[48–52] diagonal Born–Oppenheimer corrections (DBOC),[53] and post-CCSD(T) contributions[54–56]), which may need to be considered.

As the transition states on the CPES corresponding to *n*-pentane have low point-group symmetry (usually C_1), the CCSD(T) optimizations, carried out for the minima possessing higher point-group symmetry, would be exceedingly expensive. Consequently, a DFT functional suitable for replacing the coupled-cluster approach for the optimization of the reference geometries was searched for. This search was helped by a related study of Martin.[46] The performance of the DFT functionals examined is presented in detail in the Selection of the DFT functionals for the geometry optimizations section.

At this point, the notation applied during this study must be introduced. Consider a CPES, and let its global minimum be designated by $\mathcal{S}_g$, while an arbitrary structure in this space be given as $\mathcal{S}$. Then, $Q(\mathcal{S})$ indicates the value of the quantity Q computed for $\mathcal{S}$, and $\mathcal{U}(Q(\mathcal{S}))$ denotes the uncertainty of $Q(\mathcal{S})$. The relative value of $Q(\mathcal{S})$, related to $Q(\mathcal{S}_g)$ and designated by $\Delta Q(\mathcal{S})$, is

$$\Delta Q(\mathcal{S}) = Q(\mathcal{S}) - Q(\mathcal{S}_g). \tag{6}$$

If $Q_c(\mathcal{S})$ is a contribution to $Q(\mathcal{S})$, then the relative contribution is given as $\delta Q_c(\mathcal{S})$. This notation deviates from the conventional use of δ within the FPA scheme, where δ refers to energy increments. Provided that $\mathcal{R} = \mathcal{S}_1[\rightarrow \mathcal{S}_{12}] \rightarrow \mathcal{S}_2$ is an interconversion reaction from conformer $\mathcal{S}_1$ to conformer $\mathcal{S}_2$ through the transition state $\mathcal{S}_{12}$,

$$\Delta^{\ddagger}_{\mathcal{R}} Q = Q(\mathcal{S}_{12}) - Q(\mathcal{S}_1) = \Delta Q(\mathcal{S}_{12}) - \Delta Q(\mathcal{S}_1) \tag{7}$$

is the activation value of Q corresponding to $\mathcal{R}$. The activation contribution, $\delta^{\ddagger}_{\mathcal{R}} Q_c$, is expressed as

$$\delta^{\ddagger}_{\mathcal{R}} Q_c = Q_c(\mathcal{S}_{12}) - Q_c(\mathcal{S}_1) = \delta Q_c(\mathcal{S}_{12}) - \delta Q_c(\mathcal{S}_1). \tag{8}$$

When the reference structures have been chosen, the FPA approach requires single-point energy computations at these geometries. The $\Delta E(\mathcal{S})$ relative energy is decomposed here as

$$\Delta E(\mathcal{S}) = \Delta E_{HF}(\mathcal{S}) + \delta E_{MP2(fc)}(\mathcal{S}) + \delta E_{CCSD(fc)}(\mathcal{S}) + \delta E_{CCSD(T)(fc)}(\mathcal{S}) + \delta E_{CV}(\mathcal{S}), \tag{9}$$

where the so-called energy increments are

$$\delta E_{MP2(fc)}(\mathcal{S}) = \Delta E_{MP2(fc)}(\mathcal{S}) - \Delta E_{HF}(\mathcal{S}), \tag{10}$$

$$\delta E_{CCSD(fc)}(\mathcal{S}) = \Delta E_{CCSD(fc)}(\mathcal{S}) - \Delta E_{MP2(fc)}(\mathcal{S}), \tag{11}$$

$$\delta E_{CCSD(T)(fc)}(\mathcal{S}) = \Delta E_{CCSD(T)(fc)}(\mathcal{S}) - \Delta E_{CCSD(fc)}(\mathcal{S}). \tag{12}$$

In these expressions "fc" denotes the use of the frozen core approximation, while E_{HF}, $E_{MP2(fc)}$, $E_{CCSD(fc)}$, and $E_{CCSD(T)(fc)}$ are the Hartree–Fock (HF), the frozen-core second-order Møller–Plesset (MP2),[57] CCSD,[58] and CCSD(T)[59] energies, respectively. It is preferable to extrapolate these energies to the CBS limit. $\delta E_{CV}(\mathcal{S})$ includes the core-core and core-valance corrections[60] due to the prior utilization of the frozen-core approach, estimated here as follows:

$$\delta E_{CV}(\mathcal{S}) = \Delta E_{MP2(full)}(\mathcal{S}) - \Delta E_{MP2(fc)}(\mathcal{S}), \tag{13}$$

where $E_{MP2(full)}(\mathcal{S})$ is the all-electron MP2 energy. During the frozen-core computations, the 1*s* orbitals of the carbon atoms are kept frozen. In what follows "fc" will be omitted when this causes no confusion.

As to the CBS limit of the various contributions to $\Delta E(\mathcal{S})$, $\Delta E_{HF}(\mathcal{S})$, and $\delta E_\chi(\mathcal{S})$ should be extrapolated with different formulas, where $\chi \in \{MP2, CCSD, CCSD(T), CV\}$. For the relative HF energy, the following formula is utilized[61]:

$$\Delta E_{HF}(\mathcal{S}) \approx \Delta E_{HF}^{(X,X+1)}(\mathcal{S}) = \Delta E_{HF}^{[X]}(\mathcal{S}) + \frac{\Delta E_{HF}^{[X+1]}(\mathcal{S}) - \Delta E_{HF}^{[X]}(\mathcal{S})}{1 - \left(1 + \frac{1}{X+1}\right) e^{9\left(\sqrt{X} - \sqrt{X+1}\right)}}, \tag{14}$$

where $X = 2(D), 3(T), 4(Q), 5, 6, \ldots$ is the cardinal number of the Dunning-type cc-pV*X*Z basis sets,[62] $\Delta E_{HF}^{[X]}(\mathcal{S})$ is the relative HF/cc-pV*X*Z energy, and $\Delta E_{HF}^{(X,X+1)}(\mathcal{S})$ is the $(X, X+1)$ extrapolation of the HF term based on $\Delta E_{HF}^{[X]}(\mathcal{S})$ and $\Delta E_{HF}^{[X+1]}(\mathcal{S})$. The correlation contributions at the CBS limit can be estimated as[63]

$$\delta E_\chi(\mathcal{S}) \approx \delta E_\chi^{(X,X+1)}(\mathcal{S}) = \delta E_\chi^{[X]}(\mathcal{S}) + \frac{\delta E_\chi^{[X+1]}(\mathcal{S}) - \delta E_\chi^{[X]}(\mathcal{S})}{1 - \left(\frac{X}{X+1}\right)^3}, \tag{15}$$

where $\delta E_\chi^{(X,X+1)}(\mathcal{S})$ is the $(X, X+1)$ extrapolation of the χ correlation term, and X is the cardinal number of the cc-pCV*X*Z[64] and cc-pV*X*Z basis sets in the cases of $\chi = CV$ and $\chi \neq CV$, respectively.

In Refs. [27] and [29] post-CCSD(T), DBOC, and scalar relativistic[54–56] contributions were also considered. For *n*-butane and *n*-pentane, these "small corrections" seemed to cancel each other in the relative energies. Thus, these "small corrections" are neglected in the present study.

The relative zero-point vibrational energies (ZPE), responsible for about half of the uncertainties of the enthalpy differences of the conformers,[29] are computed as[65]

$$\Delta E_{\mathrm{ZPE}}(\mathcal{S})=\Delta E_{\mathrm{hZPE}}(\mathcal{S})+\delta E_{\mathrm{aZPE}}(\mathcal{S}), \tag{16}$$

with

$$\delta E_{\mathrm{aZPE}}(\mathcal{S})=\Delta E_{\mathrm{aZPE}}(\mathcal{S})-\Delta E_{\mathrm{hZPE}}(\mathcal{S}), \tag{17}$$

where $E_{\mathrm{hZPE}}(\mathcal{S})$ and $E_{\mathrm{aZPE}}(\mathcal{S})$ are the harmonic and the anharmonic ZPE, respectively. The anharmonic ZPEs are derived via hybrid degeneracy-corrected (vibrational) second-order perturbation theory (HDCPT2).[66,67]

In eq. (9), the effect of the internal rotation[68,69] should also be included. However, as the presence of hindered rotors may not affect substantially the high interconversion barriers, it was not introduced in our protocol. (During an extended future analysis, it may be worth returning to this correction.)

Interconversion parameters

To estimate the *interconversion parameters* (barrier heights, activation free energies, and rate coefficients), one should account for the energetics of the conformers and the transition states and the temperature dependence of these quantities. At a selected thermodynamic temperature T, the relative (Gibbs) free energy of the structure $\mathcal{S}$ is obtained as

$$\Delta G_T(\mathcal{S})=\Delta G_0(\mathcal{S})+\delta G_{\mathrm{corr},T}(\mathcal{S}), \tag{18}$$

where $\Delta G_0(\mathcal{S}) \equiv \Delta G_{T=0}(\mathcal{S})=\Delta E(\mathcal{S})+\Delta E_{\mathrm{ZPE}}(\mathcal{S})$, and $\delta G_{\mathrm{corr},T}(\mathcal{S})$ is the relative thermal free-energy correction provided by the formulas of statistical thermodynamics[70] within the ideal gas, rigid rotor, and harmonic oscillator approximations. (For ideal gases, $\delta G_{\mathrm{corr},T}(\mathcal{S})$ is independent of pressure.)

The rate coefficient of the reaction $\mathcal{R}=\mathcal{S}_1[\rightarrow \mathcal{S}_{12}] \rightarrow \mathcal{S}_2$ can be estimated by the aid of the Eyring–Polányi equation[71,72]:

$$k_T(\mathcal{R})=\frac{k_{\mathrm{B}}T}{h}\exp\left\{-\frac{\Delta^{\ddagger}_{\mathcal{R}}G_T}{RT}\right\}, \tag{19}$$

where k_{B} is the Boltzmann factor, R is the universal gas constant, h is the Planck constant, and $\Delta^{\ddagger}_{\mathcal{R}}G_T=\Delta G_T(\mathcal{S}_{12})-\Delta G_T(\mathcal{S}_1)$ is the activation free energy of $\mathcal{R}$. Using eqs. (9)–(18), $\Delta^{\ddagger}_{\mathcal{R}}G_T$ can be written in the following form:

$$\begin{aligned}\Delta^{\ddagger}_{\mathcal{R}}G_T=\Delta^{\ddagger}_{\mathcal{R}}E_{\mathrm{HF}}+\delta^{\ddagger}_{\mathcal{R}}E_{\mathrm{MP2}}+\delta^{\ddagger}_{\mathcal{R}}E_{\mathrm{CCSD}}+\delta^{\ddagger}_{\mathcal{R}}E_{\mathrm{CCSD(T)}}+\delta^{\ddagger}_{\mathcal{R}}E_{\mathrm{CV}}+\\ \Delta^{\ddagger}_{\mathcal{R}}E_{\mathrm{hZPE}}+\delta^{\ddagger}_{\mathcal{R}}E_{\mathrm{aZPE}}+\delta^{\ddagger}_{\mathcal{R}}G_{\mathrm{corr},T}.\end{aligned} \tag{20}$$

Given the rate coefficients, the differential mass-balance relations of the interconversion reaction networks can be solved, utilizing eqs. (9)–(12) of Ref. [73]. The kinetic behavior of these reaction networks is investigated in the Kinetic simulations section.

As indicated in the FPA approach section, the terms in the expressions of the relative energy and the activation free energy need extrapolation to both the one- and *n*-particle limits. The FPA technique is built on the fact that the higher the level of electron correlation correction the faster the convergence with respect to the expansion of the basis set. This favorable behavior helps to ensure the accuracy of the extrapolated values. Based on the convergence behavior of the one- and *n*-particle series, uncertainties can be estimated, as detailed in Table 3 (*vide infra*). It should be noted that the direct extrapolation of the terms in eq. (20) provides a better approximation for the uncertainties of $\Delta^{\ddagger}_{\mathcal{R}}G_T$ than applying the uncertainties related to $\Delta G_T(\mathcal{S}_{12})$ and $\Delta G_T(\mathcal{S}_1)$.

Selection of the DFT functionals for the geometry optimizations

As mentioned in the FPA approach section, geometry optimizations at the CCSD(T) level cannot be achieved at a reasonable computational cost. Therefore, especially for larger *n*-alkanes one must rely on the use of inexpensive DFT techniques to obtain the reference structures for the FPA analysis. Accordingly, as part of this study, an extensive search was executed for the most suitable DFT functional capable of providing the reference geometries needed for the FPA analysis.

Martin[46] obtained a 10° resolution image of the two-dimensional CPES of *n*-pentane at the CCSD(T)-F12[74] level near the CBS limit. At fixed backbone torsional angles, constrained optimizations were carried out at the CCSD(T)/cc-pVTZ and SCS-MP2/cc-pVTZ[75] levels. At these gridpoints, utilizing the cc-pVTZ basis set,[62] single-point energy computations were then performed with some wave-function-based and DFT methods free of dispersion as well as including the most popular dispersion correction schemes (-D2,[76] -D3,[77] -D3BJ[78–81], and -NL[82]). Comparing the single-point energies of the methods applied in Ref. [46] against the CCSD(T)/cc-pVTZ analogues, the DSD-PBEP86-D2[83] functional proved to be the best technique to predict the relative energies of the conformational stationary points of *n*-pentane.

In our selection procedure full geometry optimizations were performed with all the methods listed in table 1 of Ref. [46], ignoring dispersion (-noD) and including the "D2" dispersion correction scheme. These computations utilized the cc-pVTZ basis set for all the conformers of *n*-alkanes with $1 \le n_{\mathrm{C}} \le 5$. The root-mean-square deviations of the (optimally rotated and translated) geometries (GRMSD) with respect to the CCSD(T)(full)/cc-pVTZ optimized structures[27,29,84] are tabulated in Table 1 of this study. There the "total" GRMSDs ($\mathrm{GRMSD_{tot}}$), defined as

$$\mathrm{GRMSD_{tot}}=\sqrt{\sum_{i=1}^{n} n_i \mathrm{GRMSD}_i^2 / \sum_{i=1}^{n} n_i}, \tag{21}$$

are also reported, where GRMSD_i is the GRMSD of the ith structure, n_i is the number of atoms in the ith species, and n is the number of structures in Table 1.

On closer inspection of the $\mathrm{GRMSD_{tot}}$ values, it is clear that DSD-PBEP86-D2 emerges as the most accurate DFT technique for geometry optimizations. This is fully in accord with Martin's results.[46] Nevertheless, it is worth noting that ordering of the levels of theory is slightly distorted by the use of constrained geometries in Ref. [46]. For instance, MP2-noD is hardly worse

Table 1. Root-mean-square deviations of the optimized geometries (GRMSD), in mÅ, at various levels of electronic structure theory using the cc-pVTZ basis set.

Species	B2GP-PLYP-D2[85]	B2GP-PLYP-noD[85]	B3LYP-D2[76,86–88]	B3LYP-noD[87,88]	DSD-PBEP86-D2[83]	DSD-PBEP86-noD[83]	M06-2X-noD[89]	M06-noD[89]	MP2-noD	PBE0-D2[77,90]	PBE0-noD[90]	SCS-MP2-noD[75]
methane	47.7	46.7	4.0	2.2	3.0	1.5	1.1	1.2	0.4	3.8	2.9	1.0
ethane	59.6	58.7	10.6	8.3	11.2	11.2	11.5	11.6	11.9	12.4	11.0	10.9
propane	70.0	71.1	1.8	13.0	2.8	3.7	5.0	10.7	6.7	5.4	7.3	2.5
n-butane (t)	90.4	92.3	6.1	16.5	5.1	4.0	2.8	8.0	2.0	3.6	7.0	6.6
n-butane ($g^{\pm}$)	85.2	90.8	12.0	34.1	7.8	6.3	41.0	34.2	14.4	8.3	18.6	12.8
n-pentane (tt)	103.6	106.5	6.6	20.8	5.4	4.6	3.1	9.6	2.5	4.0	9.1	8.1
n-pentane ($tg^{\pm}$)	99.0	106.1	20.8	40.2	6.6	6.6	40.0	33.3	10.4	16.7	25.2	11.4
n-pentane ($g^{\pm}g^{\pm}$)	93.2	116.0	16.7	127.1	5.2	22.4	40.4	21.6	7.8	13.5	83.5	18.6
n-pentane ($g^{\pm}x^{\mp}$)	93.0	105.9	31.4	100.6	14.1	18.6	24.8	20.3	5.3	18.4	50.7	17.3
$GRMSD_{tot}$	89.1	97.1	16.6	64.8	**7.9**	12.1	27.5	21.4	**8.2**	11.8	38.9	12.3

The GRMSDs are related to the CCSD(T)(full)/cc-pVTZ equilibrium structures taken from the literature.[27,29,84]

in Table 1 of this study than DSD-PBEP86-D2, while it is only the seventh in the ranking of Ref. [46].

Following a request of one of the referees of this study, geometry optimizations have been performed using additional electronic structure theory methods free of dispersion and with those accommodating certain (-D2, -D3, and -D3BJ) dispersion schemes. To this end, both the cc-pVTZ and def2-TZVPP[91] basis sets were applied, yielding 738 optimized structures for the *n*-alkane conformers examined in Table 1. A comparison of the approximate equilibrium geometries to the CCSD(T)(full)/cc-pVTZ counterparts in terms of the $GRMSD_{tot}$ values is made in Table 2.

As seen from Table 2, there are methods comparable to DSD-PBP86-D2/cc-pVTZ in $GRMSD_{tot}$, most notably MP2-D3BJ/cc-pVTZ. However, the $GRMSD_{tot}$ values, highlighted in boldface in Table 2, exhibit only an insignificant difference. Consequently, the FPA_{eff} protocol (see An effective FPA model for describing the conformational kinetics of *n*-alkanes section), in which the DSD-PBPE86-D2/cc-pVTZ method was chosen to compute reference geometries and harmonic frequencies, appears to be an excellent and inexpensive choice for larger *n*-alkanes, as well.

Results

An effective FPA model for describing the conformational kinetics of *n*-alkanes

In this subsection, based mostly on results presented in Refs. [27] and [29], an effective FPA protocol (FPA_{eff}) is introduced for the characterization of the interconversion kinetics of *n*-alkanes. Nevertheless, to validate our novel FPA model, it is necessary to establish four auxiliary FPA schemes (FPA_{I}, FPA_{II}, $FPA_{eff(I)}$, and $FPA_{eff(II)}$), as well. Three of these procedures (FPA_{I}, FPA_{II}, and FPA_{eff}) are presented in Table 3, while the $FPA_{eff(I)}$ and $FPA_{eff(II)}$ models are derived from FPA_{eff} by substituting the DSD-PBEP86-D2/cc-pVTZ reference geometries by their CCSD(T)(full)/cc-pV*X*Z counterparts, respectively ($X=3,4$).

Although only the increments to the relative free energy are collected in Table 3, the parameters $\Delta^{\ddagger}_{\mathcal{R}}E$, $\Delta^{\ddagger}_{\mathcal{R}}G_0$, and $\Delta^{\ddagger}_{\mathcal{R}}G_T$ can also be estimated with these procedures if we introduce the quantities $\Delta^{\ddagger}_{\mathcal{R}}Q$ and $\delta^{\ddagger}_{\mathcal{R}}Q$ by analogy to $\Delta Q(\mathcal{S})$ and $\delta Q(\mathcal{S})$, respectively. Having the activation free energies determined, it is also possible to express the coefficients $k_T(\mathcal{R})$ by the aid of eq. (19) and approximate their uncertainties with the law of uncertainty propagation:

Table 2. "Total" root mean square deviations of the optimized geometries ($GRMSD_{tot}$), in mÅ, at various levels of electronic structure theory, without dispersion (-noD) and with the most common (-D2,[76] -D3,[77] and -D3BJ[78–81]) dispersion correction schemes, utilizing the cc-pVTZ and def2-TZVPP basis sets.[a]

	cc-pVTZ				def2-TZVPP			
Methods	-noD	-D2	-D3	-D3BJ	-noD	-D2	-D3	-D3BJ
B2GP-PLYP[85,92–94]	97.1	89.1	92.3	93.1	96.3	88.8	91.8	92.6
B3LYP[76,86–88,93,94]	64.8	16.6	31.3	32.6	64.2	16.1	30.6	31.8
DSD-PBEP86[83,95]	12.1	**7.9**	–	9.5	9.3	7.6	–	8.2
DSD-PBEPBE[95]	13.4	7.6	–	10.5	10.0	8.6	–	8.5
M06-2X[89,92–94]	27.5	29.2	27.1	–	27.6	29.3	27.1	–
M06[89,92–94]	21.4	24.0	20.1	–	21.8	23.6	20.8	–
MP2[92]	8.2	8.0	–	**6.5**	12.8	10.0	–	10.3
SCS-MP2[75,85]	12.3	8.8	–	–	11.7	11.7	–	–
PBE[92–94,96,97]	59.5	21.0	40.8	37.9	57.3	19.7	38.6	35.7
PBE0[77,90,92–94]	38.9	11.8	21.5	22.8	37.1	11.2	19.6	20.9
TPSS[92–94,98]	65.4	24.0	33.7	34.9	62.4	26.0	30.5	31.4
TPSS0[92–94,99]	44.3	20.2	15.6	15.6	41.9	22.2	12.8	12.9

[a] The reference equilibrium structures correspond to the CCSD(T)(full)/cc-pVTZ level.[27,29,84]

Table 3. Composition of the FPA_{eff} model and two of its ancillary FPA procedures.

	FPA_I[a]	FPA_{II}[a]	FPA_{eff}
Reference geometry	CCSD(T)/cc-pVQZ	CCSD(T)/cc-pVTZ	DSD-PBEP86-D2/cc-pVTZ
Correlation type ($\mathcal{C}$)	$\mathcal{C}$=full	$\mathcal{C}$=full	$\mathcal{C}$=fc
$\Delta E_{HF}(\mathcal{S})$	$\Delta E_{HF}^{(5,6)}(\mathcal{S})$	$\Delta E_{HF}^{(5,6)}(\mathcal{S})$	$\Delta E_{HF}^{(4,5)}(\mathcal{S})$
$\mathcal{U}(\Delta E_{HF}(\mathcal{S}))$	$\lvert\Delta E_{HF}^{(5,6)}(\mathcal{S})-\Delta E_{HF}^{(4,5)}(\mathcal{S})\rvert$	$\lvert\Delta E_{HF}^{(5,6)}(\mathcal{S})-\Delta E_{HF}^{(4,5)}(\mathcal{S})\rvert$	$\lvert\Delta E_{HF}^{(4,5)}(\mathcal{S})-\Delta E_{HF}^{(3,4)}(\mathcal{S})\rvert$
$\delta E_{MP2(\mathcal{C})}(\mathcal{S})$	$\delta E_{MP2(\mathcal{C})}^{(5,6)}(\mathcal{S})$	$\delta E_{MP2(\mathcal{C})}^{(5,6)}(\mathcal{S})$	$\delta E_{MP2(\mathcal{C})}^{(4,5)}(\mathcal{S})$
$\mathcal{U}(\delta E_{MP2(\mathcal{C})}(\mathcal{S}))$	$\lvert\delta E_{MP2(\mathcal{C})}^{(5,6)}(\mathcal{S})-\delta E_{MP2(\mathcal{C})}^{(4,5)}(\mathcal{S})\rvert$	$\lvert\delta E_{MP2(\mathcal{C})}^{(5,6)}(\mathcal{S})-\delta E_{MP2(\mathcal{C})}^{(4,5)}(\mathcal{S})\rvert$	$\lvert\delta E_{MP2(\mathcal{C})}^{(4,5)}(\mathcal{S})-\delta E_{MP2(\mathcal{C})}^{(3,4)}(\mathcal{S})\rvert$
$\delta E_{CCSD(\mathcal{C})}(\mathcal{S})$	$\delta E_{CCSD(\mathcal{C})}^{(3,4)}(\mathcal{S})$	$\delta E_{CCSD(\mathcal{C})}^{(4,5)}(\mathcal{S})$	$\delta E_{CCSD(\mathcal{C})}^{(3,4)}(\mathcal{S})$
$\mathcal{U}(\delta E_{CCSD(\mathcal{C})}(\mathcal{S}))$	$\lvert\delta E_{CCSD(\mathcal{C})}^{(3,4)}(\mathcal{S})-\delta E_{CCSD(\mathcal{C})}^{[4]}(\mathcal{S})\rvert$	$\lvert\delta E_{CCSD(\mathcal{C})}^{(4,5)}(\mathcal{S})-\delta E_{CCSD(\mathcal{C})}^{(3,4)}(\mathcal{S})\rvert$	$\lvert\delta E_{CCSD(\mathcal{C})}^{(3,4)}(\mathcal{S})-\delta E_{CCSD(\mathcal{C})}^{[4]}(\mathcal{S})\rvert$
$\delta E_{CCSD(T)(\mathcal{C})}(\mathcal{S})$	$\delta E_{CCSD(T)(\mathcal{C})}^{(3,4)}(\mathcal{S})$	$\delta E_{CCSD(T)(\mathcal{C})}^{(4,5)}(\mathcal{S})$	$\delta E_{CCSD(T)(\mathcal{C})}^{(3,4)}(\mathcal{S})$
$\mathcal{U}(\delta E_{CCSD(T)(\mathcal{C})}(\mathcal{S}))$	$\lvert\delta E_{CCSD(T)(\mathcal{C})}^{(3,4)}(\mathcal{S})-\delta E_{CCSD(T)(\mathcal{C})}^{[4]}(\mathcal{S})\rvert$	$\lvert\delta E_{CCSD(T)(\mathcal{C})}^{(4,5)}(\mathcal{S})-\delta E_{CCSD(T)(\mathcal{C})}^{(3,4)}(\mathcal{S})\rvert$	$\lvert\delta E_{CCSD(T)(\mathcal{C})}^{(3,4)}(\mathcal{S})-\delta E_{CCSD(T)(\mathcal{C})}^{[4]}(\mathcal{S})\rvert$
$\delta E_{CV}(\mathcal{S})$	0[b]	0[b]	$\delta E_{CV}^{(3,4)}(\mathcal{S})$
$\mathcal{U}(\delta E_{CV}(\mathcal{S}))$	0[b]	0[b]	$\lvert\delta E_{CV}^{(3,4)}(\mathcal{S})-\delta E_{CV}^{[4]}(\mathcal{S})\rvert$
$\Delta E_{hZPE}(\mathcal{S})$	$\Delta E_{hZPE;A}^{[3]}(\mathcal{S})$[c]	$\Delta E_{hZPE;A}^{[3]}(\mathcal{S})$[c]	$\Delta E_{hZPE;B}^{[3]}(\mathcal{S})$[d]
$\mathcal{U}(\Delta E_{hZPE}(\mathcal{S}))$	$\lvert\Delta E_{hZPE;A}^{[3]}(\mathcal{S})-\Delta E_{hZPE;A}^{[2]}(\mathcal{S})\rvert$	$\lvert\Delta E_{hZPE;A}^{[3]}(\mathcal{S})-\Delta E_{hZPE;A}^{[2]}(\mathcal{S})\rvert$	$\lvert\Delta E_{hZPE;B}^{[3]}(\mathcal{S})-\Delta E_{hZPE;B}^{[2]}(\mathcal{S})\rvert$
$\delta E_{aZPE}(\mathcal{S})$	$\delta E_{aZPE;A}(\mathcal{S})$[e]	$\delta E_{aZPE;B}(\mathcal{S})$[f]	$\delta E_{aZPE;A}(\mathcal{S})$[e]
$\mathcal{U}(\delta E_{aZPE}(\mathcal{S}))$	$\lvert\delta E_{aZPE;A}(\mathcal{S})\rvert$	$\lvert\delta E_{aZPE}(\mathcal{S})\rvert$	$\lvert\delta E_{aZPE}(\mathcal{S})\rvert$
$\delta G_{corr,T}(\mathcal{S})$	$\delta G_{corr,T;A}^{[3]}(\mathcal{S})$[g]	$\delta G_{corr,T;A}^{[3]}(\mathcal{S})$[g]	$\delta G_{corr,T;B}^{[3]}(\mathcal{S})$[h]
$\mathcal{U}(\delta G_{corr,T}(\mathcal{S}))$	$\lvert\delta G_{corr,T;A}^{[3]}(\mathcal{S})-\delta G_{corr,T;A}^{[2]}(\mathcal{S})\rvert$	$\lvert\delta G_{corr,T;A}^{[3]}(\mathcal{S})-\delta G_{corr,T;A}^{[2]}(\mathcal{S})\rvert$	$\alpha\lvert\delta G_{corr,T;B}^{[3]}(\mathcal{S})\rvert+\beta\lvert\delta G_{corr,T;B}^{[3]}(\mathcal{S})-\delta G_{corr,T;B}^{[2]}(\mathcal{S})\rvert+\gamma$[i]
$\Delta E(\mathcal{S})$	$\Delta E_{HF}(\mathcal{S})+\delta E_{MP2(\mathcal{C})}(\mathcal{S})+\delta E_{CCSD(\mathcal{C})}(\mathcal{S})+\delta E_{CCSD(T)(\mathcal{C})}(\mathcal{S})+\delta E_{CV}(\mathcal{S})$		
$\mathcal{U}(\Delta E(\mathcal{S}))$	$\mathcal{U}(\Delta E_{HF}(\mathcal{S}))+\mathcal{U}(\delta E_{MP2(\mathcal{C})}(\mathcal{S}))+\mathcal{U}(\delta E_{CCSD(\mathcal{C})}(\mathcal{S}))+\mathcal{U}(\delta E_{CCSD(T)(\mathcal{C})}(\mathcal{S}))+\mathcal{U}(\delta E_{CV}(\mathcal{S}))$		
$\Delta G_0(\mathcal{S})$	$\Delta E(\mathcal{S})+\Delta E_{hZPE}(\mathcal{S})+\delta E_{aZPE}(\mathcal{S})$		
$\mathcal{U}(\Delta G_0(\mathcal{S}))$	$\mathcal{U}(\Delta E(\mathcal{S}))+\mathcal{U}(\Delta E_{hZPE}(\mathcal{S}))+\mathcal{U}(\delta E_{aZPE}(\mathcal{S}))$		
$\Delta G_T(\mathcal{S})$	$\Delta G_0(\mathcal{S})+\delta G_{corr,T}(\mathcal{S})$		
$\mathcal{U}(\Delta G_T(\mathcal{S}))$	$\mathcal{U}(\Delta G_0(\mathcal{S}))+\mathcal{U}(\delta G_{corr,T}(\mathcal{S}))$		

[a] The FPA_I and FPA_{II} protocols are simplified versions of similar models of Refs. [27] and [29], respectively. [b] In these schemes, there is no need for the indicated correction. [c-d] $\Delta E_{hZPE;A}^{[X]}(\mathcal{S})$ and $\Delta E_{hZPE;B}^{[X]}(\mathcal{S})$ are the relative harmonic ZPE values computed at the CCSD(T)(full)/cc-pV*X*Z and DSD-PBEP86-D2/cc-pV*X*Z levels of theory (X=2, 3), respectively. [e-f] $\delta E_{aZPE;A}(\mathcal{S})$ and $\delta E_{aZPE;B}(\mathcal{S})$ are the relative anharmonic corrections determined with the MP2/6–31G* and MP2(full)/cc-pVDZ methods, respectively. [g-h] $\delta G_{corr,T;A}^{[X]}(\mathcal{S})$ and $\delta G_{corr,T;B}^{[X]}(\mathcal{S})$ are the thermal corrections to the relative free energy, computed at the CCSD(T)(full)/cc-pV*X*Z and DSD-PBEP86-D2/cc-pV*X*Z levels (X=2, 3), respectively. [i] This is an empirical formula reflecting the deviations of the FPA_{eff} estimates of the $\delta G_{corr,T}(\mathcal{S})$ values from the FPA_I/FPA_{II} results, where α=0.03, β=1.25, and γ=25 cal mol^{-1}.

$$\mathcal{U}(k_T(\mathcal{R}))=\frac{k_T(\mathcal{R})}{RT}\mathcal{U}\left(\Delta_{\mathcal{R}}^{\ddagger}G_T\right). \quad (22)$$

With the help of the auxiliary FPA models, we are able to (a) analyze the accuracy of the energy decomposition associated with the FPA_{eff} protocol and (b) gauge the magnitude of the geometry effects derived from the use of DSD-PBEP86-D2/cc-pVTZ reference structures. These investigations, detailed in Validation of the FPA_{eff} protocol against the auxiliary FPA procedures section, require (a) matching the energy increments of the FPA_I and FPA_{II} methods with their $FPA_{eff(I)}$ and $FPA_{eff(II)}$ equivalents, and (b) observing the differences of the FPA_{eff} values from the results of $FPA_{eff(I)}$ and $FPA_{eff(II)}$. Useful information can be obtained by comparing the $\Delta E_{hZPE}(\mathcal{S})$, $\Delta E_{aZPE}(\mathcal{S})$, $\delta G_{corr,T}(\mathcal{S})$ terms computed with the individual FPA procedures, as well.

All the electronic structure computations needed for the FPA analysis were performed with the Molpro 2012.1[100] and Gaussian09 release E.01[101] software packages. Molpro was utilized to determine CCSD(T) single-point energies, while Gaussian was used for all of the other quantum-chemical computations. The effects of electron correlation were computed using restricted HF orbitals, unless noted otherwise.

Validation of the FPA_{eff} protocol against the auxiliary FPA procedures

To ensure the reliability of the data obtained with the FPA_{eff} model, a comprehensive FPA analysis was carried out for the relative free energies, at 0 K, related to the conformers of *n*-butane and *n*-pentane (see Table 4). The HF relative energies converge smoothly to the CBS limit, within $\pm$1 cal mol^{-1}. The

Table 4. Convergence of the terms contributing to the relative free energies, at 0 K, for the conformers of *n*-butane and *n*-pentane using the FPA_{eff} protocol.[a,b]

$\mathcal{S}^{[c]}$	X	$\Delta E_{HF}^{[X]}(\mathcal{S})$	$\delta E_{MP2}^{[X]}(\mathcal{S})$	$\delta E_{CCSD}^{[X]}(\mathcal{S})$	$\delta E_{CCSD(T)}^{[X]}(\mathcal{S})$	$\delta E_{CV}^{[X]}(\mathcal{S})$	$\Delta E_{hZPE}^{[X]}(\mathcal{S})$	$\delta E_{aZPE}(\mathcal{S})$
$g^{\pm}$ (*n*-butane)	2	1152	−492	86	−46	4	85	–
	3	1128	−566	91	−65	2	106	–
	4	1136	−558	94	−67	2	–	–
	5	1137	−566	–	–	–	–	–
	Best[d]	1137	−575	96	−68	3	106	−4
	Unc[e]	0	23	2	1	1	21	4
$tg^{\pm}$ (*n*-pentane)	2	1186	−577	104	−58	1	90	–
	3	1184	−635	109	−75	1	106	–
	4	1194	−626	115	−77	3	–	–
	5	1195	−632	–	–	–	–	–
	Best[d]	1195	−638	118	−78	4	106	−3
	Unc[e]	0	19	3	1	1	16	3
$g^{\pm}g^{\pm}$ (*n*-pentane)	2	2368	−1399	297	−127	4	279	−17
	3	2359	−1580	312	−174	−3	314	–
	4	2378	−1574	326	−181	−1	–	–
	5	2381	−1586	–	–	–	–	–
	Best[d]	2381	−1598	337	−186	1	314	−17
	Unc[e]	1	28	11	5	2	35	17
$g^{\pm}x^{\mp}$ (*n*-pentane)	2	4335	−1286	156	−134	15	233	–
	3	4271	−1488	175	−191	17	298	–
	4	4289	−1477	191	−197	22	–	–
	5	4291	−1478	–	–	–	–	–
	Best[d]	4292	−1479	202	−202	26	298	−31
	Unc[e]	1	9	11	5	4	65	31

[a] All values are expressed in cal mol^{-1}. [b] Reference geometries were optimized at the DSD-PBEP86-D2/cc-pVTZ level of DFT theory. [c] The first column contains the torsion sequences of the conformers of *n*-butane and *n*-pentane. [d] Best estimates of the individual contributions. [e] Estimates of the uncertainties of the individual contributions.

same holds for the CCSD, CCSD(T), and CV contributions with maximum uncertainties of ±11, ±5, and ±4 cal mol^{-1}, respectively. Minor fluctuations occur in the MP2 increments, leading to larger uncertainties in the CBS values. Sextuple-ζ[102] computations providing even more accurate MP2 contributions are avoided for the reason of their considerable computational expense and as they would not improve significantly the overall accuracy of the quantities derived. The influence of the CV correction is minuscule; thus, it can be omitted from the free-energy expression.

For comparison, the FPA_{eff} protocol and its auxiliary FPA procedures were compiled to obtain the thermochemical parameters ($\Delta E(\mathcal{S})$, $\Delta G_0(\mathcal{S})$, and $\Delta G_{298}(\mathcal{S})$) describing the conformational equilibria of *n*-butane and *n*-pentane conformers. The results of our analyses are presented in Tables 5 and 6. These tables exhibit a reasonable compliance of the methods examined: the deviations of the "repeated" estimates of the individual quantities are not larger than ±100 cal mol^{-1}.

The deviations of the $FPA_{eff(I)}/FPA_{eff(II)}$ data from their FPA_I/FPA_{II} counterparts reflect the accuracy corresponding to the collection of the methods choosen in FPA_{eff}. They are largest for the MP2($\mathcal{C}$) increments, with a maximal discrepancy of ±10 cal mol^{-1}, where $\mathcal{C} \in \{\text{full}, \text{fc}\}$. As noted earlier, determining the MP2/cc-pV6Z single-point energies would imply significant increase in the computational complexity, preventing the applicability of the FPA_{eff} protocol for longer *n*-alkanes. For the $\delta E_{CCSD(\mathcal{C})}(\mathcal{S})$ and $\delta E_{CCSD(T)(\mathcal{C})}(\mathcal{S})$ parameters, the $FPA_{eff(I)}/FPA_{eff(II)}$ models provide adequate approximations: the (3,4) extrapolations differ from their fully correlated (4,5) variants by only a few cal mol^{-1}. The relative energies of the conformers are also well modeled with the $FPA_{eff(I)}/FPA_{eff(II)}$ methods, the largest deviation shown is ±37 cal mol^{-1} for the unique conformer $g^{\pm}x^{\mp}$.

As seen in Table 5, the impact of using a level less accurate than CCSD(T)(full)/cc-pVTZ for the determination of reference geometries is rather pronounced for the FPA_{eff} estimates of the $\Delta E_{HF}(\mathcal{S})$ and $\delta E_{MP2(\mathcal{C})}(\mathcal{S})$ contributions. In contrast, the FPA_{eff} values of the relative energies have discrepancies not larger than ±10 cal mol^{-1} from the results of the $FPA_{eff(I)}/FPA_{eff(II)}$ models, indicating that the geometry effects are almost totally compensated after summation of the individual terms.

Concerning the ZPE and the thermal correction terms of Table 5, the FPA_I/FPA_{II} and the FPA_{eff} values are in good agreement. While the estimated uncertainties of the $\Delta E_{hZPE}(\mathcal{S})$ parameters describe well the differences of the FPA_I/FPA_{II} and FPA_{eff} results, the uncertainties of $\delta G_{corr,\,298}(\mathcal{S})$ contributions were determined "empirically," as detailed in a footnote to Table 3. It can also be discerned from Table 5 that the rather small MP2(full)/cc-pVDZ anharmonic corrections are adequately approximated with the MP2/6-31G* quartic force field computations.

The $\Delta G_0(\mathcal{S})$ and $\Delta G_{298}(\mathcal{S})$ data provided by the various FPA models are in good agreement, demonstrating that our FPA_{eff} procedure is fairly robust; we expect that FPA_{eff} can be used for predicting the interconversion parameters of *n*-butane and

Table 5. Best estimates of the contributions to the relative free energies of the conformers of *n*-butane and *n*-pentane, at 298 K, using the FPA_{eff} protocol and its auxiliary FPA procedures.[a]

Quantity	Method	$\mathcal{S}=g^{\pm}$(*n*-butane)	$\mathcal{S}=tg^{\pm}$ (*n*-pentane)	$\mathcal{S}=g^{\pm}g^{\pm}$ (*n*-pentane)	$\mathcal{S}=g^{\pm}x^{\mp}$ (*n*-pentane)
$\Delta E_{HF}(\mathcal{S})$	FPA_I/FPA_{II}[b,c]	1109(0)	1183(0)	2363(1)[c]	4279(1)[c]
	$FPA_{eff(I)}/FPA_{eff(II)}$[b]	1109(1)	1183(0)	2362(1)[c]	4278(1)[c]
	FPA_{eff}	1137(0)	1195(0)	2381(1)	4292(1)
$\delta E_{MP2(C)}(\mathcal{S})$	FPA_I/FPA_{II}	−545(11)	−615(1)	−1580(15)	−1473(35)
	$FPA_{eff(I)}/FPA_{eff(II)}$	−541(22)	−622(19)	−1570(28)	−1464(10)
	FPA_{eff}	−575(23)	−638(19)	−1598(28)	−1479(9)
$\delta E_{CCSD(C)}(\mathcal{S})$	FPA_I/FPA_{II}	95(0)	117(5)	330(0)	199(5)
	$FPA_{eff(I)}/FPA_{eff(II)}$	96(2)	112(1)	325(11)	195(12)
	FPA_{eff}	96(2)	118(3)	337(11)	202(11)
$\delta E_{CCSD(T)(C)}(\mathcal{S})$	FPA_I/FPA_{II}	−59(0)	−80(1)	−190(2)	−204(1)
	$FPA_{eff(I)}/FPA_{eff(II)}$	−59(1)	−78(1)	−187(5)	−202(4)
	FPA_{eff}	−68(1)	−78(1)	−186(5)	−202(5)
$\delta E_{CV}(\mathcal{S})$	$FPA_{eff(I)}/FPA_{eff(II)}$	−2(0)	6(1)	6(2)	31(5)
	FPA_{eff}	3(1)	4(1)	1(2)	26(4)
$\Delta E_{hZPE}(\mathcal{S})$	FPA_I/FPA_{II}	88(0)	102(6)	319(47)	242(46)
	FPA_{eff}	106(21)	106(16)	314(35)	298(65)
$\delta E_{aZPE}(\mathcal{S})$	FPA_I/FPA_{II}	−4(4)	−6(6)	−22(22)	−28(28)
	FPA_{eff}	−4(4)	−3(3)	−17(17)	−31(31)
$\delta G_{corr,298}(\mathcal{S})$	FPA_I/FPA_{II}	−34(18)	−400(22)	232(54)	−176(94)
	FPA_{eff}	−9(31)	−423(39)	214(62)	−197(97)

[a] All values (with their uncertainties in parentheses) are given in cal mol^{-1}. [b] The FPA_I and $FPA_{eff(I)}$ methods were applied only to the $g^{\pm}$ conformer, in contrast to the FPA_{II} and $FPA_{eff(II)}$ schemes, which used only for the *n*-pentane conformers. The raw computational data needed for obtaining the best estimates of these protocols are taken from Refs. [27] and [29]. [c] The small ($\approx$ 1 cal mol^{-1}) deviations of the FPA_I/FPA_{II} and $FPA_{eff(I)}/FPA_{eff(II)}$ estimates are attributed to the use of different softwares for these computations.

n-pentane. Additionally, we also expect that larger *n*-alkanes can be modeled reliably with this FPA protocol.

Best estimates for the interconversion parameters of *n*-butane and *n*-pentane

Tables 7 and 8 demonstrate that the free energy contributions, determined via the FPA_{eff} protocol for *n*-butane and *n*-pentane, as well as the quantities derived from them have low uncertainties: the energy barriers and the free energies at 0 and 298 K have $\pm$56, $\pm$143, and $\pm$200 cal mol^{-1} maximum uncertainties, while the inaccuracy of the rate coefficients is not larger than 10%.

Inspecting the free energy contributions (Table 7), it can be seen that $\Delta^{\ddagger}_{\mathcal{R}}E_{HF}$, $\delta^{\ddagger}_{\mathcal{R}}E_{CCSD}$, and $\delta^{\ddagger}_{\mathcal{R}}E_{CCSD(T)}$ are computed with a few cal mol^{-1} uncertainties. The other terms exhibit larger uncertainties, especially $\delta^{\ddagger}_{\mathcal{R}}G_{corr,298}$, for which the maximum uncertainty is around $\pm$90 cal mol^{-1}. Table 7 also indicates that the anharmonic corrections are nearly identical for the individual reactions. As also observed in Table 5, the CV effect is not substantial: in the case of very similar geometries, the CV effect is almost completely wiped out. Most thermal correction data are about 500−600 cal mol^{-1}, due to the fact that the similar relative entropies (around 2 and 3 cal $mol^{-1}K^{-1}$ for the minima and the transition states, respectively) have significant influence on these contributions. It can also be observed that the contributions in the lower barriers have similar magnitude, in contrast to the greater activation energies, in which the correlation effects are suppressed by the $\Delta^{\ddagger}_{\mathcal{R}}E_{HF}$ factor.

As far as the energetics of the interconversions of *n*-butane and *n*-pentane is concerned (Table 8), relatively small energy barriers (less than 7 kcal mol^{-1}) are found, due to the fact that only the torsional vibrations of the conformers are excited. As a result, the interconversion processes of *n*-butane and *n*-pentane take place with rate coefficients greater than 10^7 s^{-1}. The rate coefficients cover five orders of magnitude, suggesting that certain interconversions are favored in the

Table 6. Comparison of the quantities derived from the terms listed in Table 5.

Quantity	Method	$\mathcal{S}=g^{\pm}$(*n*-butane)	$\mathcal{S}=tg^{\pm}$ (*n*-pentane)	$\mathcal{S}=g^{\pm}g^{\pm}$ (*n*-pentane)	$\mathcal{S}=g^{\pm}x^{\mp}$ (*n*-pentane)
$\Delta E(\mathcal{S})$	FPA_I/FPA_{II}	600(11)	605(7)	923(18)	2801(42)
	$FPA_{eff(I)}/FPA_{eff(II)}$	603(26)	601(22)	936(47)	2838(32)
	FPA_{eff}	593(27)	601(24)	935(47)	2839(30)
$\Delta G_0(\mathcal{S})$	FPA_I/FPA_{II}	684(15)	701(19)	1220(87)	3015(116)
	FPA_{eff}	695(49)	704(52)	1232(123)	3106(152)
$\Delta G_{298}(\mathcal{S})$	FPA_I/FPA_{II}	650(33)	301(41)	1452(141)	2839(210)
	FPA_{eff}	686(80)	281(91)	1446(185)	2909(249)

For comments, see the footnote to Table 5.

Table 7. Best estimates of the factors contributing to the activation free energies at 298 K for the gase-phase interconversions among the unique conformers of *n*-butane and *n*-pentane.[a]

	ID[b]	$\mathcal{R}$[c]	$\Delta^{\ddagger}_{\mathcal{R}}E_{HF}$	$\delta^{\ddagger}_{\mathcal{R}}E_{MP2}$	$\delta^{\ddagger}_{\mathcal{R}}E_{CCSD}$	$\delta^{\ddagger}_{\mathcal{R}}E_{CCSD(T)}$	$\delta^{\ddagger}_{\mathcal{R}}E_{CV}$	$\Delta^{\ddagger}_{\mathcal{R}}E_{hZPE}$	$\delta^{\ddagger}_{\mathcal{R}}E_{aZPE}$	$\delta^{\ddagger}_{\mathcal{R}}G_{corr,298}$
n-butane	$\mathcal{R}_1$	$t[\rightarrow \xi^{\pm}] \rightarrow g^{\pm}$	3665(1)	−238(19)	−78(5)	−52(2)	34(3)	32(49)	−16(16)	554(63)
	$\mathcal{R}_2$	$g^{\pm}[\rightarrow \xi^{\pm}] \rightarrow t$	2528(1)	337(42)	−174(3)	16(1)	31(3)	−74(28)	−12(12)	564(58)
	$\mathcal{R}_3$	$g^{\pm}[\rightarrow \tau] \rightarrow g^{\pm}$	5296(3)	−278(24)	−156(9)	−64(8)	42(3)	91(29)	−15(15)	583(60)
n-pentane	$\mathcal{R}'_1$	$tt[\rightarrow t\xi^{\pm}] \rightarrow tg^{\pm}$	3515(1)	−308(18)	−52(5)	−60(2)	29(2)	15(44)	−24(24)	212(50)
	$\mathcal{R}'_2$	$tg^{\pm}[\rightarrow t\xi^{\pm}] \rightarrow tt$	2320(1)	330(37)	−170(1)	18(1)	26(2)	−91(28)	−21(21)	635(62)
	$\mathcal{R}'_3$	$tg^{\pm}[\rightarrow g^{\pm}\xi^{\pm}] \rightarrow g^{\pm}g^{\pm}$	3332(0)	−348(24)	−18(6)	−65(3)	29(3)	23(49)	−21(21)	784(84)
	$\mathcal{R}'_4$	$g^{\pm}g^{\pm}[\rightarrow g^{\pm}\xi^{\pm}] \rightarrow tg^{\pm}$	2146(1)	612(33)	−236(1)	43(1)	32(2)	−185(31)	−8(8)	147(35)
	$\mathcal{R}'_5$	$g^{\pm}g^{\pm}[\rightarrow x^{\pm}\tau] \rightarrow g^{\pm}x^{\mp}$	6617(1)	−186(33)	−233(11)	−92(6)	56(4)	−31(67)	−21(21)	76(36)
	$\mathcal{R}'_6$	$g^{\pm}x^{\mp}[\rightarrow x^{\pm}\tau] \rightarrow g^{\pm}g^{\pm}$	4707(2)	−305(14)	−99(9)	−76(6)	31(2)	−15(37)	−7(7)	487(66)
	$\mathcal{R}'_7$	$tg^{\pm}[\rightarrow g^{\pm}\xi^{\mp}] \rightarrow g^{\pm}x^{\mp}$	3402(1)	−589(16)	37(7)	−93(3)	27(3)	50(55)	−25(25)	826(90)
	$\mathcal{R}'_8$	$g^{\pm}x^{\mp}[\rightarrow g^{\pm}\xi^{\mp}] \rightarrow tg^{\pm}$	305(2)	252(6)	−47(1)	30(0)	4(0)	−143(5)	3(3)	600(69)
	$\mathcal{R}'_9$	$g^{\pm}x^{\mp}[\rightarrow \gamma^{\pm}\gamma^{\mp}] \rightarrow g^{\pm}x^{\mp}$	124(0)	371(1)	−111(3)	34(2)	5(0)	−195(16)	−16(16)	470(80)
	$\mathcal{R}'_{10}$	$tg^{\pm}[\rightarrow t\tau] \rightarrow tg^{\pm}$	5324(5)	−395(27)	−123(11)	−84(9)	41(4)	84(27)	−18(18)	668(69)

[a] All values (with their uncertainties in parentheses) are in cal mol^{-1}. [b] Reaction identifiers (ID) are used to refer to a particular interconversion. [c] The transition states of the processes are placed in square brackets.

reaction network. As expected, the replacement of $g^{\pm}$ by $x^{\mp}$ is the slowest process, as here a change of $\pm 195^{\circ}$ occurs in one of the backbone torsion angles. Furthermore, $g^{\pm}x^{\mp} \rightarrow g^{\pm}x^{\mp}$ appears as the fastest interconversion, due to the resemblance of the reactant ($g^{\pm}x^{\mp}$) to the transition state ($\gamma^{\pm}\gamma^{\mp}$). Table 8 also reveals that the exchange of t and $g^{\pm}$ is less affected by the addition of t and $g^{\pm}$ dihedrals: $t \rightleftharpoons g^{\pm}$, $tt \rightleftharpoons tg^{\pm}$, and $tg^{\pm} \rightleftharpoons g^{\pm}g^{\pm}$, as well as $g^{\pm} \rightleftharpoons g^{\pm}$ and $tg^{\pm} \rightleftharpoons tg^{\pm}$, have very similar barrier heights. Nevertheless, the differences in the activation free energies become slightly larger due to the larger differences in entropy. It is worth noting that τ, $t\tau$, and $\gamma^{\pm}\gamma^{\mp}$ connect two isomorphic conformers on symmetric pathways; thus, their rate coefficients cannot be determined experimentally.

Comparison to previous studies

The relative energies of the conformers of *n*-butane and *n*-pentane have been subjected to a detailed analysis.[27,29] Thus, only activation free energies and energy barriers of previous studies are analyzed here. Rate coefficients for these reactions have not been found in the literature.

Tables 9 and 10 list the values for the barrier heights and the activation free energies (at 0 and 298 K) of *n*-butane and *n*-pentane. In these tables, the interconversion parameters were also computed at the DSD-PBEP86-D2/cc-pVTZ structures with those methods which are directly included in the FPA_{eff} model. In these cases, the geometry effects are not significant; thus, where larger differences occur in a given column of Tables 9 and 10, they can be attributed to the accuracy of the method applied rather than the uncertainty of the optimized geometries.

It can be observed in Table 9 that the differences are smaller for $t \rightarrow g^{\pm}$ than for $g^{\pm} \rightarrow g^{\pm}$: ± 400 and ± 1000 cal mol^{-1}, respectively. The empirical barriers are determined with the help of simple models based on the enthalpies of formation of certain *n*-alkanes[10] and on the torsional transitions of *n*-butane.[13] Note that the activation energy of $g^{\pm} \rightarrow g^{\pm}$ obtained from the latter study agrees with none of the theoretical estimates. According to Refs. [14] and [23], this is attributed to the increased uncertainty of the potential-fitting procedure used in Ref. [13].

Of the electronic structure computations listed in Table 9 the protocol followed in this study involves the most elaborate

Table 8. Best estimates of the reaction parameters (energy barriers, activation free energies at 0 and 298 K, and rate coefficients at 298 K) for the gase-phase interconversions of *n*-butane and *n*-pentane.[a]

	ID	$\Delta^{\ddagger}_{\mathcal{R}}E$ (cal mol^{-1})	$\Delta^{\ddagger}_{\mathcal{R}}G_0$ (cal mol^{-1})	$\Delta^{\ddagger}_{\mathcal{R}}G_{298}$ (cal mol^{-1})	$k_{298}(\mathcal{R})$ (s^{-1})
n-butane	$\mathcal{R}_1$	3331(30)	3347(95)	3901(158)	$103(7) \times 10^7$
	$\mathcal{R}_2$	2738(50)	2652(90)	3216(148)	$33(2) \times 10^8$
	$\mathcal{R}_3$	4840(47)	4916(91)	5499(151)	$69(4) \times 10^6$
n-pentane	$\mathcal{R}'_1$	3124(28)	3115(96)	3327(146)	$27(2) \times 10^8$
	$\mathcal{R}'_2$	2524(42)	2412(91)	3047(153)	$44(3) \times 10^8$
	$\mathcal{R}'_3$	2930(36)	2932(106)	3716(190)	$14(1) \times 10^8$
	$\mathcal{R}'_4$	2597(38)	2404(77)	2551(112)	$101(5) \times 10^8$
	$\mathcal{R}'_5$	6162(55)	6110(143)	6186(179)	$22(2) \times 10^6$
	$\mathcal{R}'_6$	4258(33)	4236(77)	4723(143)	$26(1) \times 10^7$
	$\mathcal{R}'_7$	2784(30)	2809(110)	3635(200)	$16(1) \times 10^8$
	$\mathcal{R}'_8$	544(9)	404(17)	1004(86)	$137(5) \times 10^9$
	$\mathcal{R}'_9$	423(6)	212(38)	682(118)	$24(1) \times 10^{10}$
	$\mathcal{R}'_{10}$	4763(56)	4829(101)	5497(170)	$69(5) \times 10^6$

[a] The reaction IDs are defined in Table 7.

Table 9. Energy barriers and activation free energies at 298 K reported by various studies for the gase-phase interconversions of *n*-butane.[a,f]

Quantity	$\mathcal{R}_1$[b]	$\mathcal{R}_3$[b]	Method[d]	Ref.[c]
$\Delta^{\ddagger}_{\mathcal{R}}E$	3720	5400	Empirical	[10]
	3620	3277	Empirical	[13]
	3320	5210	MP3/6–311G**//MP2/6–31G	[11]
	3400	5380	MP3/6–31+G*//MP2/6–31G*	[12]
	3539	5196	CBS/Q	[14]
	3294	5196	G2	
	3310 {3298}[d]	4890 {4883}[d]	CCSD(T)/cc-pVTZ//MP2/6–311G(2df,p)	[15]
	3307	4876	CCSD(T)/CBS//CISD/DZP	[16]
	3246	4833	B3LYP/6–311G**//B3LYP/6–311G**	[17]
	3303 {3292}[d]	– {4817}[d]	MP2:CC//MP2/cc-pVDZ	[18]
	3428 {3422}[d]	– {5039}[d]	MP2/cc-pVQZ//MP2/cc-pVDZ	
	3356	–	C27r//MP2/cc-pVDZ	
	3345	–	C27//MP2/cc-pVDZ	
	3880	–	AMBER99//MP2/cc-pVDZ	
	3643 {3650}[d]	5329 {5323}[d]	MP2/cc-pVDZ//MP2/cc-pVDZ	[21]
	3517 {3521}[d]	5125 {5119}[d]	CCSD(T)/cc-pVDZ//MP2/cc-pVDZ	
	3430 {3422}[d]	5036 {5039}[d]	MP2/cc-pVQZ//MP2/cc-pVDZ	
	3303 {3292}[d]	4832 {4817}[d]	MP2:CC//MP2/cc-pVDZ	
	3100	4600	DFT (potential fitting)	[23]
	3440	5100	MP2/6–31G*//MP2/6–31G*	[28]
	3331(30)	4840(47)	FPA_{eff} (see the text)	This study
$\Delta^{\ddagger}_{\mathcal{R}}G_{298}$	4080	5820	CBS/Q	[14]
	3830	5820	G2	
	3971 {3884}[d,e]	5450 {5601}[d,e]	CCSD(T)/cc-pVTZ//MP2/6–311G(2df,p)	[15]
	3901(158)	5499(151)	FPA_{eff} (see the text)	This study

[a] All values are given in cal mol^{-1}. [b] The reaction IDs are defined in Table 7. [c] The line numbers of the sources are listed here. [d] Values in braces were obtained with the methods detailed in the 4th column of this table at the DSD-PBEP86-D2 reference geometries. [e] These numbers were computed using the thermal free energy corrections of the present FPA_{eff} protocol. For details on the methods, see the original papers.

quantum-chemical techniques, as far as the reference geometries, the basis sets, and the levels of the single-point energy computations are considered. One can recognize that certain studies (see, e.g., Ref. [11]) give a good approximation of the energy barrier for the conversion $t \rightarrow g^{\pm}$, but fail to predict correctly the barrier height for the reaction $g^{\pm} \rightarrow g^{\pm}$. In those cases where a 100 cal mol^{-1} deviation of a particular datum from our FPA_{eff} estimates is observed, the electron correlation effects were computed at relatively high levels. As to $\Delta^{\ddagger}_{\mathcal{R}}G_{298}$, the literature values agree well with the present FPA_{eff} estimate for the reaction $t \rightarrow g^{\pm}$. As to $g^{\pm} \rightarrow g^{\pm}$, the impact of hindered rotors, which was taken into account in Ref. [14], may be the reason behind the larger differences from our FPA_{eff} estimates, where the internal rotation effects are not considered.

For *n*-pentane, no experimental or empirical studies are available. Of the computational investigations (see Table 10), the results of Ref. [46] agree very well with our FPA_{eff} estimates: the absolute differences are within or near to the uncertainties provided by the present protocol. The inexpensive molecular mechanics force field results, applied in Ref. [18], show larger discrepancies, around $\pm$1000 cal mol^{-1} in the worst case. Combination of the MP2/cc-pVDZ, MP2/cc-pVQZ, and CCSD(T)/cc-pVDZ energies, denoted as MP2:CC, provides a good estimation for the barrier heights. Although this does not affect the correctness of the computations in Ref. [18], we must note that Klauda et al.[18] improperly designated the conformer $g^{+}x^{-}$ as $g^{+}g^{-}$: the second torsion angle is $\approx -95^{\circ}$ instead of $\approx -60^{\circ}$. The results in Table 10 also suggest that the MP2/6–31G* method overcorrects the effect of electron correlation, both for the barrier heights and for the activation free energies. This overestimation is likely due to intramolecular basis set superposition error (BSSE).

Kinetic simulations

Next, sequences of interconversions corresponding to *n*-butane and *n*-pentane are investigated, based on the theory of first-order complex reaction networks (FCRN).[73,103] Due to the fact that these reaction networks include components (unique conformers) less than six (in fact, two and four), their first-order linear system of ordinary differential equations (FLSODE) can be given in an algebraically closed form.[73,103]

Consider a general FCRN containing K components. For a general case, the FLSODE of this reaction network can be expressed as follows:

$$\dot{\mathbf{C}} = \mathbf{F}\mathbf{C}, \tag{23}$$

where $\mathbf{C}=\mathbf{C}(t)$ is the vector of size K including the time-dependent concentrations of the components, $\dot{\mathbf{C}}$ is the time derivative of $\mathbf{C}$, and $\mathbf{F}$ is a $K \times K$ matrix constructed from the rate coefficients. If $\mathbf{C}_0=\mathbf{C}(t=0)$ is the vector of initial concentrations and $\lambda_1, \lambda_2, \ldots, \lambda_L$ are pairwise distinct (not necessarily real) eigenvalues of $\mathbf{F}$ with corresponding $\mu_1, \mu_2, \ldots, \mu_L$ multiplicities, $\mathbf{C}=\mathbf{C}(t)$ can be given as[73,103]

Table 10. Energy barriers ($\Delta^{\ddagger}_{\mathcal{R}}E$) and activation free energies at 0 K ($\Delta^{\ddagger}_{\mathcal{R}}G_0$) reported by various studies for the gase-phase interconversions of *n*-pentane.[a,c,e]

Quantity	$\mathcal{R}'_1$	$\mathcal{R}'_3$	$\mathcal{R}'_5$	$\mathcal{R}'_7$	$\mathcal{R}'_9$	$\mathcal{R}'_{10}$	Method[a]	Ref.
$\Delta^{\ddagger}_{\mathcal{R}}E$	3396	3185	6859	3093	362	5329	MP2/6–31G*//MP2/6–31G*	[1]
	3200[c] {3095}	2892 {2889}	– {6108}	2764 {2758}	– {427}	– {4746}	MP2:CC//MP2/cc-pVDZ	[18]
	3213 {3204}	2971 {2972}	– {6429}	2819 {2813}	– {490}	– {4945}	MP2/cc-pVQZ//MP2/cc-pVDZ	
	2946	2935	–	2965	–	–	C27r//MP2/cc-pVDZ	
	3329	3407	–	3297	–	–	C27//MP2/cc-pVDZ	
	3910	3845	–	3636	–	–	AMBER99//MP2/cc-pVDZ	
	3106 {3103}	2898 {2896}	6138 {6133}	2769 {2767}	407 {403}	4800 {4797}	CCSD(T)/cc-pVTZ//**c**CCSD(T)/cc-pVTZ	[46]
	3106 {3103}	2899 {2896}	6140 {6133}	2770 {2767}	406 {403}	4800 {4797}	CCSD(T)/cc-pVTZ//**c**SCS-MP2/cc-pVTZ	
	3100	2892	6096	2754	421	4740	CCSD(T)-F12/cc-pVDZ-F12//**c**SCS-MP2/cc-pVTZ	
	3098	2893	6119	2752	423	4740	CCSD(T)-F12/cc-pVTZ-F12//**c**SCS-MP2/cc-pVTZ	
	3098	2894	6118	2751	426	4739	CCSD(T)-F12/cc-pVTZ-F12//**c**CCSD(T)/cc-pVTZ	
	3124(28)	2930(36)	6162(55)	2784(30)	423(6)	4763(56)	FPA_{eff} (see text)	This study
$\Delta^{\ddagger}_{\mathcal{R}}G_0$	3402	3190	6783	3124	187	5382	MP2/6–31G*//MP2/6–31G*	[1]
	3115(96)	2932(106)	6110(143)	2809(110)	212(38)	4829(101)	FPA_{eff} (see text)	This study

All values are given in cal mol^{-1}. [a] The letter "c" in boldface indicates the use of constrained optimization. [b] Values in braces were obtained with the methods of the 8th column at the DSD-PBEP86-D2 reference geometries. [c] This datum shows an unusually large discrepancy from the value in braces. After trying to reproduce this number, we determined 3105 cal mol^{-1} instead of 3200 cal mol^{-1}. [d] For further comments, see the footnote to Table 9.

$$\mathbf{C}(t)=\mathbf{F}_{\mathbf{C}_0}\mathbf{V}^{-1}\mathbf{E}(t), \tag{24}$$

where

$$\mathbf{E}(t)=\{e^{\lambda_1 t}, te^{\lambda_1 t}, \ldots, t^{\mu_1-1}e^{\lambda_1 t}, e^{\lambda_2 t}, te^{\lambda_2 t}, \ldots, t^{\mu_2-1}e^{\lambda_2 t}, .., e^{\lambda_L t}, te^{\lambda_L t}, \ldots, t^{\mu_L-1}e^{\lambda_L t}\}^{\mathsf{T}}, \tag{25}$$

$$\mathbf{V}=\left\{\mathbf{E}(0), \dot{\mathbf{E}}(0), \ddot{\mathbf{E}}(0), \ldots, \mathbf{E}^{(K-1)}(0)\right\}, \tag{26}$$

and

$$\mathbf{F}_{\mathbf{C}_0}=\{\mathbf{C}_0, \mathbf{F}\mathbf{C}_0, \mathbf{F}^2\mathbf{C}_0, \ldots, \mathbf{F}^{K-1}\mathbf{C}_0\}, \tag{27}$$

with the vector $\mathbf{E}^{(k)}(0)=\left(\mathrm{d}^{(k)}\mathbf{E}(t)/\mathrm{d}t^k\right)_{t=0}$ and the transpose operation T. The eigenvalues of **F** can be determined by solving $p_{\mathbf{F}}(\lambda)=0$, where $p_{\mathbf{F}}(\lambda)$ is the characteristic polynomial of **F**:

$$p_{\mathbf{F}}(\lambda)=a_{K+1}\lambda^K+a_K\lambda^{K-1}+\ldots+a_2\lambda+a_1. \tag{28}$$

The coefficients of $p_{\mathbf{F}}(\lambda)$ can be obtained with the help of Leverrier's method[73,103]:

$$a_{K+1}=(-1)^K, \tag{29}$$

$$a_{K+1-k}=-\frac{1}{k}\sum_{i=1}^{k}a_{K+1-k+i}\mathrm{tr}\left(\mathbf{F}^i\right)\ (1\le k\le K), \tag{30}$$

where $\mathrm{tr}\left(\mathbf{F}^i\right)$ is the trace of the *i*th power of **F**.

The FLSODE induced by the interconversion mechanism of *n*-butane in eq. (3) is a system of two differential mass-balance relations, namely

$$\begin{aligned}\dot{c}_{\mathrm{t}}&=-k_1c_{\mathrm{t}}+k_2c_{\mathrm{g}^{\pm}}\\ \dot{c}_{\mathrm{g}^{\pm}}&=k_1c_{\mathrm{t}}-k_2c_{\mathrm{g}^{\pm}}=-\dot{c}_{\mathrm{t}},\end{aligned} \tag{31}$$

where (a) $k_1=k_{298}(\mathcal{R}_1)$ and $k_2=k_{298}(\mathcal{R}_2)$, following the notation of Table 5; (b) $c_{\mathrm{t}}=c_{\mathrm{t}}(t)$ and $c_{\mathrm{g}^{\pm}}=c_{\mathrm{g}^{\pm}}(t)$ are the time-dependent concentration functions of species t and $\mathrm{g}^{\pm}$, respectively; and (c) $\dot{c}_{\mathrm{t}}$ and $\dot{c}_{\mathrm{g}^{\pm}}$ are the time derivatives of c_{t} and $c_{\mathrm{g}^{\pm}}$, respectively. Obviously, the reversible reaction $\mathrm{g}^{\pm}\rightleftharpoons\mathrm{g}^{\pm}$ is canceled out in eq. (31); thus, $k_{298}(\mathcal{R}_3)$ does not occur in this equation. For this FLSODE, the vectors and matrices of eqs. (24)–(27) can be written as follows:

$$\mathbf{C}=\left\{c_{\mathrm{t}}, c_{\mathrm{g}^{\pm}}\right\}^{\mathsf{T}}, \tag{32}$$

$$\mathbf{C}_0=\left\{c_{0,\mathrm{t}}, c_{0,\mathrm{g}^{\pm}}\right\}^{\mathsf{T}}, \tag{33}$$

$$\mathbf{F}=\begin{pmatrix}-k_1 & k_2\\ k_1 & -k_2\end{pmatrix}, \tag{34}$$

$$\mathbf{E}(t)=\left\{e^{\lambda_1 t},\ e^{\lambda_2 t}\right\}^{\mathsf{T}}=\left\{1,\ e^{-(k_1+k_2)t}\right\}^{\mathsf{T}}, \tag{35}$$

$$\mathbf{V}=\left\{\mathbf{E}(0),\ \dot{\mathbf{E}}(0)\right\}=\begin{pmatrix}1 & 0\\ 1 & -k_1-k_2\end{pmatrix}, \tag{36}$$

$$\mathbf{F}_{\mathbf{C}_0}=\{\mathbf{C}_0,\ \mathbf{F}\mathbf{C}_0\}=\begin{pmatrix}c_{0,\mathrm{t}} & k_2c_{0,\mathrm{g}^{\pm}}-k_1c_{0,\mathrm{t}}\\ c_{0,\mathrm{g}^{\pm}} & k_1c_{0,\mathrm{t}}-k_2c_{0,\mathrm{g}^{\pm}}\end{pmatrix}, \tag{37}$$

where $\lambda_1=0$ and $\lambda_2=-k_1-k_2$ are the eigenvalues of the matrix **F** in eq. (34). Substituting eqs. (32)–(37) into eq. (24), the solution of eq. (23) can be obtained by performing the matrix inversion and the multiplications in eq. (24).

n-butane is not an easily resolvable mixture of its conformers, which exist in thermodynamic equilibrium at a given temperature and pressure. Thus, the experimental preparation of a non-equilibrium initial state at constant temperature for the species t and $\mathrm{g}^{\pm}$ is not trivial. A feasible solution to this problem was suggested by Zwier,[34] whose idea, called IR-induced population transfer, builds on the fact that individual conformers can be excited in a conformation-specific way. For instance, if conformer t is excited, then the equilibrium concentrations, $c_{\infty\mathrm{t}}$ and $c_{\infty\mathrm{g}^{\pm}}$, will be perturbed with Π to $c_{\infty,\mathrm{t}}-\Pi$ and $c_{\infty,\mathrm{g}^{\pm}}+\Pi$, respectively. From the $\mathbf{C}_0=\left\{c_{\infty,\mathrm{t}}-\Pi, c_{\infty,\mathrm{g}^{\pm}}+\Pi\right\}^{\mathsf{T}}$

initial state, the system will return to equilibrium following first-order kinetics. At 298 K, $c_{\infty t}$ and $c_{\infty g^{\pm}}$ can be expressed as

$$\frac{c_{\infty,g^{\pm}}}{c_{\infty,t}}=\frac{k_1}{k_2}, \tag{38}$$

$$c_{tot}=c_{\infty,t}+c_{\infty,g^{\pm}}, \tag{39}$$

where c_{tot} is the total concentration of *n*-butane. After some algebraic manipulations,

$$c_{\infty,t}=\frac{k_2 c_{tot}}{k_1+k_2} \tag{40}$$

and

$$c_{\infty,g^{\pm}}=c_{tot}-c_{\infty,t}. \tag{41}$$

Using $c_{tot}=1$ mol dm^{-3} and $\Pi=0.2c_{\infty,t}$, 0.61 and 0.39 mol dm^{-3} are obtained for $c_{0,t}$ and $c_{0,g^{\pm}}$, respectively, which serve as the initial parameters of our simulation depicted in Figure 3. The uncertainties of the concentrations were determined via a Monte-Carlo uncertainty analysis,[104] based on 1000 simulations. During this process, the rate coefficients were varied within their uncertainty intervals, while the initial concentrations were treated as exact, to better represent the effects caused by the inaccuracy of the rate coefficients on the kinetic model considered. It can be proved that these uncertainty estimates are identical for $c_t(t)$ and $c_{g^{\pm}}(t)$, as shown in Figure 3. It can also be seen there that the uncertainties are increasing up to equilibrium. The largest uncertainty of the concentrations is not larger than 10%.

For the interconversion network of *n*-pentane in eq. (5), the following first-order system of differential equations can be constructed:

$$\begin{aligned}
\dot{c}_{tt}&=-k'_1c_{tt}+k'_2c_{tg^{\pm}}\\
\dot{c}_{tg^{\pm}}&=k'_1c_{tt}-(k'_2+k'_3+k'_7)c_{tg^{\pm}}+k'_4c_{g^{\pm}g^{\pm}}+k'_8c_{g^{\pm}x^{\mp}}\\
\dot{c}_{g^{\pm}g^{\pm}}&=k'_3c_{tg^{\pm}}-(k'_4+k'_5)c_{g^{\pm}g^{\pm}}+k'_6c_{g^{\pm}x^{\mp}}\\
\dot{c}_{g^{\pm}x^{\mp}}&=k'_7c_{tg^{\pm}}+k'_5c_{g^{\pm}g^{\pm}}-(k'_6+k'_8)c_{g^{\pm}x^{\mp}},
\end{aligned} \tag{42}$$

where (a) $k'_i=k_{298}(\mathcal{R}'_i)$ $(1\le i\le 8)$ following the notation of Table 5, and (b) c_{tt}, $c_{tg^{\pm}}$, $c_{g^{\pm}g^{\pm}}$, and $c_{g^{\pm}x^{\mp}}$ are the concentration functions of the species tt, tg$^{\pm}$, g$^{\pm}$g$^{\pm}$, and g$^{\pm}$x$^{\mp}$, respectively. As observed in the case of *n*-butane, the reactions between two isomorphic conformers do not appear in the differential mass balance relations. The coefficient matrix of this reaction network is

$$\mathbf{F}=\begin{pmatrix}
-k'_1 & k'_2 & 0 & 0\\
k'_1 & -(k'_2+k'_3+k'_7) & k'_4 & k'_8\\
0 & k'_3 & -(k'_4+k'_5) & k'_6\\
0 & k'_7 & k'_5 & -(k'_6+k'_8)
\end{pmatrix}. \tag{43}$$

When the eigenvalues of **F**, which can be determined via the Cardano formula, are available, the solution of eq. (42) is provided by eqs. (24)–(27). To make a simulation for this reaction network, $\mathbf{C}_0=\left\{c_{\infty,tt}-\Pi, c_{\infty,tg^{\pm}}+\Pi, c_{\infty,g^{\pm}g^{\pm}}, c_{\infty,g^{\pm}x^{\mp}}\right\}^{T}$ is used, where

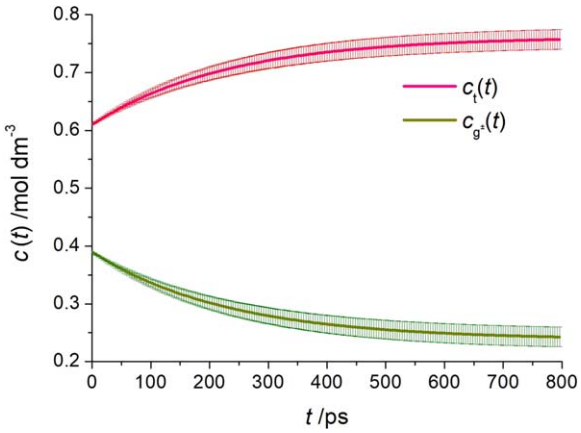

Figure 3. Concentration profiles corresponding to the interconversion network of *n*-butane. To obtain the uncertainty intervals shown, only the uncertainties of the rate coefficients were taken into account. [Color figure can be viewed at wileyonlinelibrary.com]

$$c_{\infty,tg^{\pm}}=\frac{k'_1}{k'_2}c_{\infty tt}, \tag{44}$$

$$c_{\infty,g^{\pm}g^{\pm}}=\frac{k'_3}{k'_4}c_{\infty,tg^{\pm}}=\frac{k'_1}{k'_2}\frac{k'_3}{k'_4}c_{\infty,tt}, \tag{45}$$

$$c_{\infty,g^{\pm}x^{\mp}}=\frac{k'_5}{k'_6}c_{\infty,g^{\pm}g^{\pm}}=\frac{k'_1}{k'_2}\frac{k'_3}{k'_4}\frac{k'_5}{k'_6}c_{\infty,tt}, \tag{46}$$

and

$$c_{\infty,tt}=\frac{c_{tot}}{1+\frac{k'_1}{k'_2}+\frac{k'_1}{k'_2}\frac{k'_3}{k'_4}+\frac{k'_1}{k'_2}\frac{k'_3}{k'_4}\frac{k'_5}{k'_6}}, \tag{47}$$

with $c_{tot}=1$ mol dm^{-3} and $\Pi=0.5c_{\infty,tt}$.

The concentration curves of Figure 4 were obtained with the help of these parameters, following the same procedure

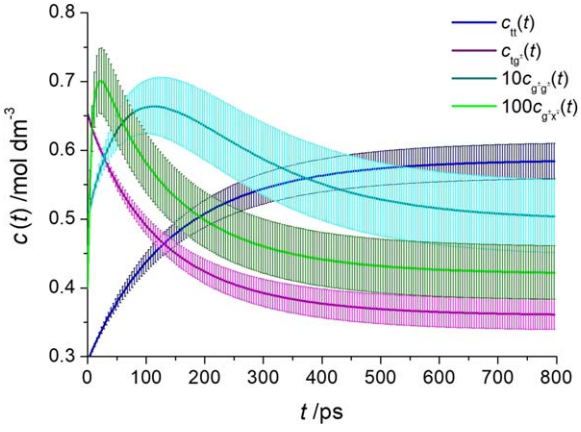

Figure 4. Concentration profiles corresponding to the interconversion network of *n*-pentane. To obtain the uncertainty intervals shown, only the uncertainties of the rate coefficients were taken into account. [Color figure can be viewed at wileyonlinelibrary.com]

applied for the interconversion network of *n*-butane. As seen in Figure 4, the concentrations of the species $g^{\pm}g^{\pm}$ and $g^{\pm}x^{\mp}$ are rather small, around $0.1c_{\infty,tt}$ and $0.01c_{\infty,tt}$, respectively. The Monte-Carlo uncertainties of these components are nearly 10%, which are greater than the uncertainties related to tt and $tg^{\pm}$, about 4.5 and 6%, respectively.

Based on all this information, the estimated parameters of our FPA_{eff} model describing the interconversions of *n*-butane and *n*-pentane can be considered dependable. To improve the uncertainties of the concentrations of $g^{\pm}g^{\pm}$ and $g^{\pm}x^{\mp}$, mainly the ZPEs should be computed even more accurately, following more sophisticated models and methods with a larger computational cost.

Conclusions

A FPA model, denoted by FPA_{eff}, was presented to estimate the conformational interconversion parameters of two *n*-alkanes, *n*-butane, and *n*-pentane. In accordance with a recommendation of Martin,[46] the DSD-PBEP86-D2 level of DFT theory was used for geometry optimizations and harmonic frequency computations, which can safely substitute the reference structures and the harmonic frequencies obtained at the much more expensive CCSD(T)(full)/cc-pVTZ level. The accuracy of the estimated energy barriers, activation free energies, and rate coefficients for the interconversions of *n*-butane and *n*-pentane conformers is ensured by a sequence of single-point energy computations at high levels of electronic structure theory. For all of our data, rather small and always reliable uncertainties are provided. Comparing our FPA_{eff} estimates against the corresponding values of previous quantum-chemical investigations, of which the present FPA_{eff} procedure emerges as the most extensive protocol for predicting the interconversion parameters of unbranched alkanes, a good agreement is found with results of MP theory and of coupled-cluster techniques. Although at present experimental studies dealing with the kinetic behavior of these reaction systems are not available, they could be useful for benchmarking this as well as future computational studies. The current FPA_{eff} scheme is recommended for modeling the interconversion parameters of longer *n*-alkanes, as well.

Acknowledgments

Discussions with Dr. Julien Bloino and Professor György Lendvay on some of the topics of this paper are gratefully acknowledged. Dr. Balázs Nagy and Dr. József Csontos are thanked for sending the computational results of Refs. [27] and [29]. We would also like to express our gratitude to Professor J. M. L. Martin for providing technical assistance in using DFT functionals for geometry optimizations.

Keywords: focal-point analysis · thermochemistry · *n*-alkanes · interconversion rate coefficients · uncertainty analysis

How to cite this article: R. Tóbiás, A. G. Császár, L. Gyevi-Nagy, G. Tasi. *J. Comput. Chem.* **2018**, *39*, 424–437. DOI: 10.1002/jcc.25130

Additional Supporting Information may be found in the online version of this article.

[1] G. Tasi, B. Nagy, G. Matisz, T. S. Tasi, *Comput. Theor. Chem.* **2011**, *963*, 378.
[2] J. H. Jensen, M. S. Gordon, *J. Am. Chem. Soc.* **1991**, *113*, 7917.
[3] S. Stepanian, I. Reva, E. Radchenko, L. Adamowicz, *J. Phys. Chem. A* **1998**, *102*, 4623.
[4] E. Czinki, A. G. Császár, *Chem. Eur. J.* **2003**, *9*, 1008.
[5] V. Kasalová, W. D. Allen, H. F. Schaefer, E. Czinki, A. G. Császár, *J. Comput. Chem.* **2007**, *28*, 1373.
[6] T. Szidarovszky, G. Czakó, A. G. Császár, *Mol. Phys.* **2009**, *107*, 761.
[7] J. J. Wilke, M. C. Lind, H. F. I. Schaefer, A. G. Császár, W. D. Allen, *J. Chem. Theory Comput.* **2009**, *5*, 1511.
[8] H. M. Jaeger, H. F. Schaefer, III, J. Demaison, A. G. Császár, W. D. Allen, *J. Chem. Theory Comput.* **2010**, *6*, 3066.
[9] Z. A. Tehrani, E. Tavasoli, A. Fattahi, *J. Mol. Struct. (Theochem)* **2010**, *960*, 73.
[10] K. Ito, *J. Am. Chem. Soc.* **1953**, *75*, 2430.
[11] K. Raghavachari, *J. Chem. Phys.* **1984**, *81*, 1383.
[12] K. B. Wiberg, M. A. Murcko, *J. Am. Chem. Soc.* **1988**, *110*, 8029.
[13] W. Herrebout, B. Van der Veken, A. Wang, J. Durig, *J. Phys. Chem.* **1995**, *99*, 578.
[14] M. A. Murcko, H. Castejon, K. B. Wiberg, *J. Phys. Chem.* **1996**, *100*, 16162.
[15] G. D. Smith, R. L. Jaffe, *J. Phys. Chem.* **1996**, *100*, 18718.
[16] N. L. Allinger, J. T. Fermann, W. D. Allen, H. F. I. Schaefer, *J. Chem. Phys.* **1997**, *106*, 5143.
[17] P. Vansteenkiste, V. Van Speybroeck, G. Marin, M. Waroquier, *J. Phys. Chem. A* **2003**, *107*, 3139.
[18] J. B. Klauda, B. R. Brooks, A. D. MacKerell, R. M. Venable, R. W. Pastor, *J. Phys. Chem. B* **2005**, *109*, 5300.
[19] G. Tarczay, T. A. Miller, G. Czakó, A. G. Császár, *Phys. Chem. Chem. Phys.* **2005**, *7*, 2881.
[20] G. Tasi, R. Izsák, G. Matisz, A. G. Császár, M. Kállay, B. Ruscic, J. F. Stanton, *ChemPhysChem* **2006**, *7*, 1664.
[21] M. J. Hafezi, F. Sharif, *J. Mol. Struct. (Theochem)* **2007**, *814*, 43.
[22] G. Czakó, E. Mátyus, A. C. Simmonett, A. G. Császár, H. F. Schaefer, W. D. Allen, *J. Chem. Theory Comput.* **2008**, *4*, 1220.
[23] E. E. Santiso, M. Buongiorno Nardelli, K. E. Gubbins, *J. Chem. Phys.* **2008**, *128*, 034704.
[24] R. M. Balabin, *J. Phys. Chem. A* **2009**, *113*, 1012.
[25] G. Czakó, B. Nagy, G. Tasi, Á. Somogyi, J. Šimunek, J. Noga, B. J. Braams, J. M. Bowman, A. G. Császár, *Int. J. Quantum Chem.* **2009**, *109*, 2393.
[26] C. R. Kemnitz, J. L. Mackey, M. J. Loewen, J. L. Hargrove, J. L. Lewis, W. E. Hawkins, A. F. Nielsen, *Chem. Eur. J.* **2010**, *16*, 6942.
[27] D. Barna, B. Nagy, J. Csontos, A. G. Császár, G. Tasi, *J. Chem. Theory Comput.* **2012**, *8*, 479.
[28] M. Stojanović, J. Aleksić, M. Baranac-Stojanović, *Tetrahedron* **2015**, *71*, 5119.
[29] J. Csontos, B. Nagy, L. Gyevi-Nagy, M. Kállay, G. Tasi, *J. Chem. Theory Comput.* **2016**, *12*, 2679.
[30] K. N. Kirschner, W. Heiden, D. Reith, *Mol. Phys.* **2017**, *115*, 1155.
[31] B. C. Dian, A. Longarte, T. S. Zwier, *Science* **2002**, *296*, 2369.
[32] B. C. Dian, J. R. Clarkson, T. S. Zwier, *Science* **2004**, *303*, 1169.
[33] B. C. Dian, G. M. Florio, J. R. Clarkson, A. Longarte, T. S. Zwier, *J. Chem. Phys.* **2004**, *120*, 9033.
[34] T. S. Zwier, *J. Phys. Chem. A* **2006**, *110*, 4133.
[35] N. C. Polfer, J. Oomens, *Phys. Chem. Chem. Phys.* **2007**, *9*, 3804.
[36] T. M. Selby, T. S. Zwier, *J. Phys. Chem. A* **2007**, *111*, 3710.
[37] T. A. LeGreve, J. R. Clarkson, T. S. Zwier, *J. Phys. Chem. A* **2008**, *112*, 3911.
[38] N. R. Pillsbury, C. W. Müller, T. S. Zwier, *J. Phys. Chem. A* **2009**, *113*, 5013.
[39] N. R. Pillsbury, T. S. Zwier, *J. Phys. Chem. A* **2009**, *113*, 126.

[40] A. L. Burin, S. L. Tesar, V. M. Kasyanenko, I. V. Rubtsov, G. I. Rubtsov, *J. Phys. Chem. C* **2010**, *114*, 20510.
[41] Allen, W. D., East, A. L. L., Császár, A. G. In *Structures and Conformations of Non-Rigid Molecules*; J. Laane, M. Dakkouri, B. van der Veken, H. Oberhammer, Eds.; Kluver: Dortrecht, The Netherlands, **1993**; pp. 343–373.
[42] A. G. Császár, W. D. Allen, H. F. I. Schaefer, *J. Chem. Phys.* **1998**, *108*, 9751.
[43] G. Tasi, F. Mizukami, *J. Math. Chem.* **1999**, *25*, 55.
[44] G. Tasi, F. Mizukami, J. Csontos, W. Győrffy, I. Pálinkó, *J. Math. Chem.* **2000**, *27*, 191.
[45] E. L. Eliel, N. L. Allinger, S. J. Angyal, G. A. Morrison, *Conformational Analysis*; Interscience: New York, **1965**.
[46] J. M. L. Martin, *J. Phys. Chem. A* **2013**, *117*, 3118.
[47] H. Chung, B. Braams, K. Bartschat, A. G. Császár, G. Drake, T. Kirchner, V. Kokoouline, J. Tennyson, *J. Phys. D: Appl. Phys.* **2016**, *49*, 363002.
[48] M. Douglas, N. M. Kroll, *Ann. Phys.* **1974**, *82*, 89.
[49] B. A. Hess, *Phys. Rev. A* **1986**, *33*, 3742.
[50] G. Tarczay, A. G. Császár, W. Klopper, H. M. Quiney, *Mol. Phys.* **2001**, *99*, 1769.
[51] M. Reiher, A. Wolf, *J. Chem. Phys.* **2004**, *121*, 2037.
[52] M. Reiher, A. Wolf, *J. Chem. Phys.* **2004**, *121*, 10945.
[53] J. Gauss, A. Tajti, M. Kállay, J. F. Stanton, P. G. Szalay, *J. Chem. Phys.* **2006**, *125*, 144111.
[54] M. Kállay, J. Gauss, *J. Chem. Phys.* **2005**, *123*, 214105.
[55] Y. J. Bomble, J. F. Stanton, M. Kállay, J. Gauss, *J. Chem. Phys.* **2005**, *123*, 054101.
[56] M. Kállay, J. Gauss, *J. Chem. Phys.* **2008**, *129*, 144101.
[57] C. Møller, M. S. Plesset, *Phys. Rev.* **1934**, *46*, 618.
[58] G. D. Purvis, III, R. J. Bartlett, *J. Chem. Phys.* **1982**, *76*, 1910.
[59] K. Raghavachari, G. W. Trucks, J. A. Pople, M. Head-Gordon, *Chem. Phys. Lett.* **1989**, *157*, 479.
[60] A. G. Császár, W. D. Allen, *J. Chem. Phys.* **1996**, *104*, 2746.
[61] G. Tasi, A. G. Császár, *Chem. Phys. Lett.* **2007**, *438*, 139.
[62] T. H. Dunning, Jr., *J. Chem. Phys.* **1989**, *90*, 1007.
[63] T. Helgaker, W. Klopper, H. Koch, J. Noga, *J. Chem. Phys.* **1997**, *106*, 9639.
[64] D. E. Woon, T. H. Dunning, Jr., *J. Chem. Phys.* **1995**, *103*, 4572.
[65] I. M. Mills, In *Molecular Spectroscopy: Modern Research*; K. N. Rao, C. W. Mattiews, Eds.; Academic Press: New York, NY, **1972**.
[66] J. Bloino, M. Biczysko, V. Barone, *J. Chem. Theory Comput.* **2012**, *8*, 1015.
[67] M. Piccardo, J. Bloino, V. Barone, *Int. J. Quantum Chem.* **2015**, *115*, 948.
[68] G. Ercolani, *J. Chem. Educ.* **2000**, *77*, 1495.
[69] J. Pfaendtner, X. Yu, L. J. Broadbelt, *Theor. Chem. Acc.* **2007**, *118*, 881.
[70] D. A. McQuarrie, J. D. Simon, *Molecular Thermodynamics*; University Science Books: Sausalito, CA, **1999**.
[71] H. Eyring, *J. Chem. Phys.* **1935**, *3*, 107.
[72] M. G. Evans, M. Polanyi, *Trans. Faraday Soc.* **1935**, *31*, 875.
[73] R. Tóbiás, G. Tasi, *J. Math. Chem.* **2016**, *54*, 85.
[74] G. Knizia, T. B. Adler, H.-J. Werner, *J. Chem. Phys.* **2009**, *130*, 054104.
[75] S. Grimme, *J. Chem. Phys.* **2003**, *118*, 9095.
[76] S. Grimme, *J. Comput. Chem.* **2006**, *27*, 1787.
[77] S. Grimme, J. Antony, S. Ehrlich, H. Krieg, *J. Chem. Phys.* **2010**, *132*, 154104.
[78] A. Koide, *J. Phys. B: At., Mol. Opt. Phys.* **1976**, *9*, 3173.
[79] A. D. Becke, E. R. Johnson, *J. Chem. Phys.* **2005**, *123*, 154101.
[80] E. R. Johnson, A. D. Becke, *J. Chem. Phys.* **2006**, *124*, 174104.
[81] A. D. Becke, E. R. Johnson, *J. Chem. Phys.* **2007**, *127*, 154108.
[82] O. A. Vydrov, T. Van Voorhis, *J. Chem. Phys.* **2010**, *133*, 244103.
[83] S. Kozuch, J. M. Martin, *Phys. Chem. Chem. Phys.* **2011**, *13*, 20104.
[84] R. D. Johnson, *NIST Computational Chemistry Comparison and Benchmark Database*. Available at: http://srdata.nist.gov/cccbdb, accessed on October 10, **2017**.
[85] A. Karton, A. Tarnopolsky, J.-F. Lamere, G. C. Schatz, J. M. Martin, *J. Phys. Chem. A* **2008**, *112*, 12868.
[86] S. Grimme, *J. Comput. Chem.* **2004**, *25*, 1463.
[87] A. D. Becke, *Phys. Rev. A* **1988**, *38*, 3098.
[88] A. D. Becke, *J. Chem. Phys.* **1993**, *98*, 5648.
[89] Y. Zhao, D. G. Truhlar, *Theor. Chem. Acc.* **2008**, *120*, 215.
[90] C. Adamo, V. Barone, *J. Chem. Phys.* **1999**, *110*, 6158.
[91] F. Weigend, R. Ahlrichs, *Phys. Chem. Chem. Phys.* **2005**, *7*, 3297.
[92] B. Brauer, M. K. Kesharwani, S. Kozuch, J. M. Martin, *Phys. Chem. Chem. Phys.* **2016**, *18*, 20905.
[93] S. Grimme, *List of Functionals and Coefficients for Zero-Damping*. Available at: https://www.chemie.uni-bonn.de/pctc/mulliken-center/software/dft-d3/functionals, accessed on October 10, **2017**.
[94] S. Grimme, *List of Functionals and Coefficients for BJ-Damping*. Available at: https://www.chemie.uni-bonn.de/pctc/mulliken-center/software/dft-d3/functionalsbj, accessed on October 10, **2017**.
[95] S. Kozuch, J. M. Martin, *J. Comput. Chem.* **2013**, *34*, 2327.
[96] J. P. Perdew, K. Burke, M. Ernzerhof, *Phys. Rev. Lett.* **1996**, *77*, 3865.
[97] J. Perdew, K. Burke, *Phys. Rev. Lett.* **1997**, *78*, 1396.
[98] J. Tao, J. P. Perdew, V. N. Staroverov, G. E. Scuseria, *Phys. Rev. Lett.* **2003**, *91*, 146401.
[99] S. Grimme, *J. Phys. Chem. A* **2005**, *109*, 3067.
[100] H.-J. Werner, P. J. Knowles, G. Knizia, F. R. Manby, M. Schütz, *Wiley Interdiscip. Rev. Comput. Mol. Sci.* **2012**, *2*, 242.
[101] M. J. Frisch, G. W. Trucks, H. B. Schlegel, G. E. Scuseria, M. A. Robb, J. R. Cheeseman, G. Scalmani, V. Barone, B. Mennucci, G. A. Petersson, H. Nakatsuji, M. Caricato, X. Li, H. P. Hratchian, A. F. Izmaylov, J. Bloino, G. Zheng, J. L. Sonnenberg, M. Hada, M. Ehara, K. Toyota, R. Fukuda, J. Hasegawa, M. Ishida, T. Nakajima, Y. Honda, O. Kitao, H. Nakai, T. Vreven, J. A. Montgomery, Jr., J. E. Peralta, F. Ogliaro, M. Bearpark, J. J. Heyd, E. Brothers, K. N. Kudin, V. N. Staroverov, R. Kobayashi, J. Normand, K. Raghavachari, A. Rendell, J. C. Burant, S. S. Iyengar, J. Tomasi, M. Cossi, N. Rega, J. M. Millam, M. Klene, J. E. Knox, J. B. Cross, V. Bakken, C. Adamo, J. Jaramillo, R. Gomperts, R. E. Stratmann, O. Yazyev, A. J. Austin, R. Cammi, C. Pomelli, J. W. Ochterski, R. L. Martin, K. Morokuma, V. G. Zakrzewski, G. A. Voth, P. Salvador, J. J. Dannenberg, S. Dapprich, A. D. Daniels, Ö. Farkas, J. B. Foresman, J. V. Ortiz, J. Cioslowski, D. J. Fox, *Gaussian 09, Revision E.01*; Gaussian, Inc.: Wallingford, CT, **2009**. Available at: http://www.gaussian.com, accessed on October 10, 2017.
[102] A. K. Wilson, T. van Mourik, T. H. Dunning, *J. Mol. Struct. (Theochem)* **1996**, *388*, 339.
[103] R. Tóbiás, L. L. Stacho, G. Tasi, *J. Math. Chem.* **2016**, *54*, 1863.
[104] K. Mosegaard, M. Sambridge, *Inverse Probl.* **2002**, *18*, R29.

Received: 8 August 2017
Revised: 27 October 2017
Accepted: 31 October 2017
Published online on 14 December 2017